

Numeričko modeliranje procesa deformiranja poroznog kućišta konektora

Tomić, Zoran

Master's thesis / Diplomski rad

2019

Degree Grantor / Ustanova koja je dodijelila akademski / stručni stupanj: **University of Zagreb, Faculty of Mechanical Engineering and Naval Architecture / Sveučilište u Zagrebu, Fakultet strojarstva i brodogradnje**

Permanent link / Trajna poveznica: <https://urn.nsk.hr/urn:nbn:hr:235:504882>

Rights / Prava: [In copyright](#)/[Zaštićeno autorskim pravom.](#)

Download date / Datum preuzimanja: **2025-03-29**

Repository / Repozitorij:

[Repository of Faculty of Mechanical Engineering and Naval Architecture University of Zagreb](#)



UNIVERSITY OF ZAGREB
FACULTY OF MECHANICAL ENGINEERING AND NAVAL
ARCHITECTURE

MASTER'S THESIS

Zoran Tomić

Zagreb, 2019

UNIVERSITY OF ZAGREB
FACULTY OF MECHANICAL ENGINEERING AND NAVAL
ARCHITECTURE

MASTER'S THESIS

Mentor:

Prof. dr. sc. Zdenko Tonković

Student:

Zoran Tomić

Zagreb, 2019

Izjavljujem da sam ovaj rad izradio samostalno koristeći znanja stečena tijekom studija i navedenu literaturu.

Zahvala (Acknowledgment)

Na samom početku, hvala kolegi Anti Bubalu, mag.ing.mech. iz tvrtke Yazaki Europe Ltd. podružnica Zagreb, na susretljivosti i utrošenom vremenu tijekom pisanja ovoga rada. Hvala na svim testovima, savjetima i pristupačnosti.

Zahvala i svim ostalim kolegama, djelatnicima i vodstvu tvrtke Yazaki Europe Ltd, Zagreb.

Hvala doc. dr. sc. Tomislavu Lesičaru na neiscrpnim idejama tijekom mnogobrojnih sastanaka. Posebno hvala za sve savjete tijekom numeričkog dijela istraživanja.

Osobito se želim zahvaliti mentoru, prof. dr. sc. Zdenku Tonkoviću. Hvala na ukazanom povjerenju od samog početka. Jednostavnost, pristupačnost tijekom i van radnog vremena, optimizam te ugodna i pozitivna atmosfera tijekom svih sastanaka i razgovora ostavili su trajan utisak.

Hvala mojim prijateljima s fakulteta. Svakodnevne kave su trenuci koji će ostati u sjećanju.

Za nepresušni izvor smijeha, bezuvjetne podrške i iskrene ljubavi,
velika zahvala svim mojim prijateljima (sve i do jednom!),
osobito njima iz Vitamina i Fegareta.

Iz svakog diferencijalnog elementa moga bića, vječna zahvala mojoj sestri Ilijani te mojim roditeljima, Mirku i Ljubici. Hvala im.

Zoran Tomić



SVEUČILIŠTE U ZAGREBU
FAKULTET STROJARSTVA I BRODOGRADNJE



Središnje povjerenstvo za završne i diplomske ispite
Povjerenstvo za diplomske ispite studija strojarstva za smjerove:
procesno-energetski, konstrukcijski, brodstrojarski i inženjersko modeliranje i računalne simulacije

| | |
|--|--------|
| Sveučilište u Zagrebu Fakultet strojarstva i brodogradnje | |
| Datum | Prilog |
| Klasa: | |
| Ur. broj: | |

DIPLOMSKI ZADATAK

Student: **Zoran Tomić**

Mat. br.: 0035202746

Naslov rada na hrvatskom jeziku: **Numeričko modeliranje procesa deformiranja poroznog kućišta konektora**

Naslov rada na engleskom jeziku: **Numerical Modelling of Deformation Processes of Porous Connector Housing**

Opis zadatka:

Yazaki Corporation designs, develops, produces, and sells specialized automotive connectors and terminals. A connector housing for an automobile in which wire harnesses and terminal fittings are incorporated, is injection-moulded of a resin. The Polybutylene terephthalate (PBT) is frequently used as a moulding material of a connector housing due to its excellent mechanical and electrical properties as well as heat and water resistance. To reduce the size and thickness of the connector housings, fibres such as glass fibres are added to the PBT to increase the strength and stiffness of the component. However, during the injection moulding process of the PBT, defects such as porosities can occur within the PBT material, degrading the stiffness and strength of the component.

This master thesis will investigate the influence of porosity on the response of the unreinforced and glass fibre-reinforced PBT as well as the strength of the connector housing. Based on everything said above in this study it is necessary to:

1. Study available literature on the modelling of material behaviour by using the Direct Numerical Simulation (DNS) in which the heterogeneities from the micro scale are explicitly modelled in the macro scale model.
2. Determine the influence of the material volume element size on the predicted effective response of unreinforced and glass fibre-reinforced PBT material consisting of various porosity ratio, using the DNS and appropriate boundary conditions. Here, the realistic material microstructure should be modelled by using information obtained from the 3D X-ray micro-Computed Tomography imaging technique.
3. Validate the numerical results by comparison with the experimental measurements.
4. Estimate the mechanical response of the connector housing with various amounts of porosities.

During thesis preparation one must comply with the standard rules for preparation of master thesis. It is necessary to list all literature used and received assistance.

Zadatak zadan:

26. rujna 2019.

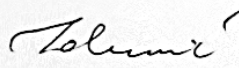
Datum predaje rada:

28. studenoga 2019.

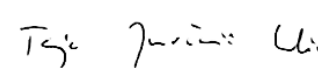
Predvideni datum obrane:

2. – 6. prosinca 2019.

Zadatak zadao:


Prof. dr. sc. Zdenko Tonković

Predsjednica Povjerenstva:


Prof. dr. sc. Tanja Jurčević Lulić

CONTENTS

| | |
|---|------|
| LIST OF FIGURES | III |
| LIST OF TABLES | V |
| LIST OF SYMBOLS | VI |
| LIST OF ABBREVIATIONS | VII |
| PROŠIRENI SAŽETAK..... | VIII |
| ABSTRACT | X |
| | |
| 1. Introduction | 1 |
| 1.1. Motivation | 2 |
| 1.2. Thesis overview | 3 |
| 2. Theoretical background..... | 5 |
| 2.1. Polymeric materials | 5 |
| 2.1.1. Polybutylene terephthalate – PBT | 5 |
| 2.2. <i>Hydrocerol</i> | 7 |
| 2.3. Injection moulding | 8 |
| 2.4. Computed tomography..... | 10 |
| 2.4.1. Historical overview of computed tomography | 10 |
| 2.4.2. Physical basics of CT technology..... | 12 |
| 2.4.3. Image reconstruction..... | 13 |
| 3. Mechanical behaviour of investigated materials | 18 |
| 3.1. Direct numerical simulation | 18 |
| 3.2. Mechanics of heterogeneous materials [30]..... | 20 |
| 4. Experimental testing | 23 |

| | |
|---|----|
| 4.1. Hydrocerol impact to mechanical properties | 23 |
| 5. Numerical testing..... | 27 |
| 5.1. CT models | 31 |
| 6. Mechanical response of the connector housing..... | 35 |
| 6.1. Experimental testing of CPA..... | 36 |
| 6.2. Numerical results of the CPA..... | 37 |
| 7. Discussion | 42 |
| 8. CONCLUSION | 47 |

LIST OF FIGURES

| | |
|---|----|
| Figure 1. Influence of increasing short glass fiber share on mechanical response of polymeric (PBT) composite [9]..... | 6 |
| Figure 2. Injection moulding design rules and advices [9]..... | 9 |
| Figure 3. Irregularity on injection moulded component gained by CT, a) 2D section view, b) location on component..... | 9 |
| Figure 4. Types of CT scanners according to size of a focal point depending on resolution and measuring range [20]..... | 13 |
| Figure 5. Voxel as a part of reconstructed volume [20] | 14 |
| Figure 6. Principle of 2D planar X Ray beam. attenuation of an X Ray which passes through an object is measured on 1D detector for two different angles θ_1 i θ_2 [19]..... | 14 |
| Figure 7. Number of projections influence onto quality of reconstructed image. with big amount of projections FBP is very efficient [19] | 16 |
| Figure 8.. Example of surface determination using threshold value, a) real image, b) ideal image [20] | 16 |
| Figure 9.. Variation in diameter measurements of a cylindrical part for different threshold values. The diameter is calculated using an ideal cylindrical surface to the resulting CT point cloud. [20] | 17 |
| Figure 10. Typical histogram of scanned testing probe..... | 20 |
| Figure 11. Idealized stress/strain curve of a polymer under uniaxial tension in x-direction..... | 21 |
| Figure 12. Dimensions of standard ISO 527 testing sample..... | 23 |
| Figure 13. CT slice of testing sample. Change of density under influence of hydrocerol chemical blowing agent is visible in form of greyvalue variation | 24 |
| Figure 14. The testing setup: the testing machine and the experimental sample positioned respectively..... | 25 |
| Figure 15. Results from four groups of experimental samples with different manufacturing techniques | 26 |

| | |
|--|----|
| Figure 16. Experimental results for different PBT samples with hydrocerol additive in comparison with pure PBT sample. Significant deviation in results is visible for samples | 26 |
| Figure 17. Set of models with irregularities in form of pores. Models contain 2% of randomly placed pores with size of 500nm..... | 27 |
| Figure 18. Result comparison with different size RVEs | 28 |
| Figure 19. Different RVE size models. RVE model groups with: a) unidirectional fibre placement and b) random placement. | 29 |
| Figure 20. Comparison results from DNS analysis for different RVE size models from: a) unidirectional RVE group, b) random RVE group | 30 |
| Figure 21. a) 3D model of experimental sample obtained by CT scan, b) cross section of scanned sample | 31 |
| Figure 22. a) Cross section of full model with voids, b) large model, c) medium model, d) small model..... | 32 |
| Figure 23. Void inside the volume, a) before smoothing feature, b) after smoothing feature..... | 32 |
| Figure 24. Boundary conditions applied on models | 33 |
| Figure 25. Comparison between different sizes RVEs and experimental test | 34 |
| Figure 26. Yazaki connector housing with appropriate connector positioning assurance | 35 |
| Figure 27. Connector positioning assurance (CPA) of the connector housing | 36 |
| Figure 28. Experimental setup where connectors CPA is tested | 36 |
| Figure 29. Experimental results of CPA | 37 |
| Figure 30. The CT DNS model of an ROI of housing CPA with boundary conditions and loading | 38 |
| Figure 31. Deformed shape of the ROI of investigated CPA | 38 |
| Figure 32. Comparison results between CPA experimental test and the DNS of the ROI based on CT scans | 39 |
| Figure 33. CPA slice. Deleting the pixels in slice in order to create pores | 40 |
| Figure 34. Porous DNS model. Porosities are located close to critical section | 40 |
| Figure 35. Comparison results for the different percentages of porosities in the critical section of the CPA component | 41 |

LIST OF TABLES

| | |
|--|----|
| Table 1. Mechanical properties of PBT [7] | 6 |
| Table 2. Sample groups and manufacturing description | 25 |
| Table 3. Size and FE number for different unreinforced RVE models | 28 |
| Table 4. Size and FE number for different fibre reinforced RVE models..... | 29 |
| Table 5. Different size of RVE models from CT scan with information of elements and voids number..... | 33 |
| Table 6. DNS models with different porosities..... | 40 |

LIST OF SYMBOLS

| <i>Symbol</i> | | <i>Symbol description</i> | | <i>Unit</i> |
|---------------|---|---------------------------|---|-------------|
| E | - | photon energy | - | J |
| h | - | Planck constant | - | Js |
| f | - | frequency | - | Hz |
| c | - | speed of light | - | m/s |
| λ | - | wavelength of X-rays | - | m |
| μ | - | attenuation | - | [-] |
| I | - | X-ray intensity | - | eV |
| b | - | absorption | - | Gy |
| D | - | object thickness | - | m |

LIST OF ABBREVIATIONS

| | | |
|-------|---|--|
| 2D | - | two-dimensional |
| 3D | - | three-dimensional |
| CAD | - | computer aided design |
| CPA | - | connector positioning assurance |
| CT | - | computed tomography |
| DICOM | - | Digital Imaging and Communications in Medicine |
| DNS | - | direct numerical simulation |
| DOF | - | degree of freedom |
| FBP | - | filtered back projection |
| FE | - | finite element |
| HU | - | Hounsfield units |
| NDT | - | nondestructive testing |
| PBT | - | Polybutylene terephthalate |
| RVE | - | representative volume element |

PROŠIRENI SAŽETAK

Cilj rada bio je istražiti utjecaj poroznosti na mehaničko ponašanje polimernog materijala polibutilen tereftalata (PBT-a) koji spada u grupu (polu-) kristalnih polimera, odnosno poliester termoplastika. PBT se najčešće koristi u električnoj industriji za proizvodnju konektora i prekidača te ostalih komponenata električne industrije gdje je potrebno zadovoljiti stroge norme i propise. Kada govorimo o automobilskoj industriji, PBT se može pronaći na gotovo svim mjestima automobila, od odbojnika, ručica vrata pa sve do električnih konektora kao što je slučaj u tvrtki Yazaki Europe Ltd. Iako PBT posjeduje zavidna mehanička svojstva, nerijetko se dodatno poboljšava ojačanjem u vidu staklenih vlakana.

U ovom radu provedeno je numeričko modeliranje i računalna simulacija procesa deformiranja PBT-a ojačanog staklenim vlaknima kao i čistog PBT-a bez ojačanja vlaknima.

Za modeliranje mikrostrukture primijenjena je direktna numerička simulacija (engl. *Direct Numerical Simulation*; u daljnjem tekstu DNS) s modelima dobivenim primjenom 3D mikrorračunalne tomografije X-zrakama (*3D X-ray micro-Computed tomography* (μ -CT)). Prije provedbe analiza dana je teorijska pozadina vezana za tehnologiju računalne tomografije, kratki opis korištenih materijala te DNS metoda. Pojam DNS odnosi se na provođenje detaljnim numeričkih simulacija ponašanja materijala pri čemu se eksplicitno modelira mikrostruktura materijala bez upotrebe višerazinskih simulacija koje uključuju homogenizacijske procedure i definiranje reprezentativnog volumenskog elementa (RVE) materijala. Pritom treba identificirati minimalno potrebnu veličinu modela te istražiti utjecaj rubnih uvjeta na vanjskim plohama modela na deformiranje uzorka materijala.

Prvi dio rada bavi se istraživanjem utjecaja veličine RVE modela na mehaničko ponašanje PBT-a. Istraživanje je provedeno na 3D modelima akademskih primjera materijala i modelima dobivenim preko mikro CT tehnologije. Također, analizirane su različite veličine RVE modela čistog PBT materijala i vlaknima ojačanog PBT-a. Nakon

što su numeričke analize provedene na akademskim modelima, istražen je utjecaj veličine RVE modela s CT snimki. Numeričke analize validirane su koristeći odgovarajuće eksperimentalne testove. U tu svrhu, izvršeni su jednoosni testovi na kidalici i to na uzorcima sa i bez staklenih vlakana.

U drugom dijelu rada provedena je numerička analiza naprezanja u standardnom električnom konektoru za automobilsku industriju. Numeričke analize provedene su na CT modelu osigurača konektora, poznatijem kao CPA (engl. *Connector Positioning Assurance*) a rezultati su validirani eksperimentalnim testom. Također, istražen je utjecaj poroznosti na mehaničko ponašanje CPA komponente konektora. Na modelima s mikro CT-a isprovocirane su pore te su uspoređeni rezultati s različitim udjelom poroznosti.

Na kraju rada izrađena je diskusija gdje su prokomentirani svi rezultati. Isto tako, potencijalna poboljšanja numeričkih modela, a i budući rad prikazan je na kraju rada.

Ključne riječi: polibutilen tereftalat (PBT), metoda konačnih elemenata, direktna numerička simulacija (DNS), mikroročunalna tomografija X-zrakama (mikro CT), reprezentativni volumenski element (RVE), električni konektor

ABSTRACT

The main goal was to investigate porosity influence on mechanical behaviour of the polymer material, the polybutylene terephthalate (PBT) which belongs to the group of (semi-) crystal polymers, or polyester thermoplastics. PBT is often used in electrical industry for connector and plug switches and other components of electrical industry where strict regulations and standards are present. When dealing with automotive industry, PBT can be founded in all sections of the car, from bumpers, handles to electrical connectors, like the one company Yazaki designs and produces. Even though PBT has envious mechanical properties, very often PBT is additionally glass fibre reinforced.

In this thesis, numerical modelling and computer simulations of deformation process are carried out with the glass fibre reinforced and the unreinforced PBT samples.

For the microstructure modelling, direct numerical simulation (DNS) is applied on the models based on micro X-ray computed tomography (μ -CT, or CT). Before the analyses, theoretical background of the CT technology is given, along with mechanics of used material and DNS method. The term DNS is usually referred to detail numerical simulations of the heterogeneous materials during which microstructure is directly modelled without multilevel simulations including homogenisation procedures and defining representative volume element (RVE) of a material. During this process, RVE size must be determined and boundary conditions on external surfaces must be investigated for appropriate model deformation.

The first part of the thesis is dealing with research on different RVE sizes and their connection with mechanical behaviour. The research is conducted on academic based RVE models and CT gained models. Different sizes of pure PBT samples, along with glass fibre reinforced samples are simulated, respectively. After the research on academic-based models, CT based RVEs are also analysed. Numerical results are validated using appropriate experimental tests. For these purposes, uniaxial experimental tests are conducted on pure and glass-fibre reinforced PBT testing samples.

The second part of the thesis deals with investigation of the stress analysis in standard electrical connector for automotive industry. Numerical simulations are conducted on a CT based model of the connector position assurance (CPA) component. Numerical results are then compared with experimental tests. Influence of porosities on CPA mechanical behaviour is investigated. On the CT based models, pores are modelled in different percentages and results are compared afterwards.

At the end of the thesis, results are discussed. Potential improvements and future work are given.

Key words: Polybutylene terephthalate (PBT), finite element method, direct numerical simulation (DNS), micro X-ray computed tomography, representative volume element (RVE), electrical connector

1. Introduction

The automotive industry is one of the biggest markets of today's world, third to be exact, right after the finance and oil industry [1]. So, it's not surprising, that even today, after decades of development, an enormous amount of money is invested in research and development of cars. Encouraged by strong electrification revolution, it's not surprising even bigger demand of components necessary for electric energy transmission, and other components that go with it.

The main goal of car industry is the weight reduction, and therefore energy-saving, so it's crucial that all components have mass as low as possible. Use of polymer materials is a great way to reduce weight. Car components can be created using a different kind of manufacturing technologies, and one of the most important manufacturing technologies in the car industry is the technology of injection moulding where hot melted material is injected under high pressure into the tool that has shape of a final product.

In recent decades fibre-reinforced polymeric materials are widely accepted by European car-industry for different kinds of car components [2]. An increase in mechanical properties along with weight reduction is one of the most important tasks of today's automotive industry.

Development of component's complexity is also an even bigger challenge for today's engineers. Production of these components is faced with increased complexity problems mostly because of mechanical and market demands [3]. Design complexity is limited mostly with manufacturing technologies. Since design complexity development is much faster than technology development itself, there are often component imperfections that occur and thereby reduction of demanded mechanical properties.

The imperfections of polymeric components created by injection moulding, are manifested through holes inside of a part. Because of the different wall thickness, very often the latter imperfections are located at a considerable change of a cross section. To reduce the phenomenon of volume imperfections, guidelines are introduced in a design point of view.

When imperfections have occurred, it's important to know what kind of influence they have on mechanical behaviour.

That's why, in order to study the influence of imperfections, in the last few years in the automotive industry, advanced computer tomography is introduced. This nondestructive testing method allows very detailed and clear insight to surface condition but also the condition inside of a part (whole volume). Using ionizing radiation, this NDT method remains only technology that is capable of detecting and measuring, not only surface imperfections but also a volume imperfections that are not visible from outside [4]. The massive potential of computerized tomography in the industry is noticed in the late 80s. A huge development explains almost doubled yearly income in 2017 in comparison with 2011 [4].

Considering that data from tomography are saved as a huge number of slices, it's possible to extract a region of interest (ROI) in the form of the point cloud. In this kind of form, it's possible to show scanned object using finite elements and perform numerical simulations. Unlike the medical application of tomography, the industry allows the application of much higher energy, and therefore the much finer resolution is possible ($\sim 10\mu\text{m}$).

This research is conducted in collaboration with Yazaki Europe Ltd. – branch office Zagreb.

1.1. Motivation

The car-industry puts weight as the most interesting feature in the goal of making lightweight and energy-efficient vehicles. That's why even the greatest car manufacturers are turning to polymeric materials wherever they can. From the other side, computed tomography in industrial application its roots owe directly to the automotive industry.

This join of advanced technology it's capable of analyzing the real components with all its flaws. Unlike ideal CAD models, models gain by tomography are including all irregularities of a surface as well as volume defects.

Numerical analyses in recent years have greater significance so experimental testings, because of saving time and money, are increasingly avoiding where possible. But in order to validate numerical results, it's crucial to run experimental tests and compare them with numerical results.

Introduction of numerical analysis using models from tomography would reduce the need for experimental tests, and more importantly, results from this kind of analysis are much closer to real experimental results then the results gained by CAD models. Since this kind of numerical simulation is a relatively new, it's important to investigate different kinds of possibilities and reduce all problems that occur during the transformation of tomography model to numerical one.

Because of all mentioned above, it's crucial to determine differences of mechanical behaviour using CAD models and models from tomography. With these findings, it's possible to predict the life span of the component much better and realistically closer to experimental results than using numerical results from CAD models.

1.2. Thesis overview

The main goal of this thesis is to give an overview of numerical results using CAD models in comparison with models gained by CT and compare these results with experimental tests. Previously, the problem overview, that is being addressed, is given. Afterwards in chapter two theoretical background of computerized tomography is described. Also, the used materials, technology of injection moulding and other steps used in this thesis are described. Besides that, the mathematical description of polymeric material and fibre-reinforced material behaviour is given using material models.

In third chapter, an overview of the experimental test is given. The uniaxial quasi-static experimental tests are conducted on test samples with irregularities in order to validate the numerical results. Besides the test samples, the real components - the connectors, are numerically and experimentally tested and validated.

In 4th chapter, the process of getting numerical models from tomography images is described. The theoretical background of numerical models along with results is given.

In the end, in chapter 5, results are compared and discussed along with used methods. Future improvements and disadvantages are given.

2. Theoretical background

2.1. Polymeric materials

In the light of lightweight structures, polymeric materials along lightweight metallic materials are fighting for their position in automotive industry. Mechanical property of polymeric materials is depending on manufacturing process and loading conditions and, even if the chemical composition is the same, polymeric creation can manifest differences regarding shape and position of polymeric chains at molecular level [5].

For purpose of this thesis PBT polymer is used. Mechanical characteristics and properties are described in following chapters.

2.1.1. Polybutylene terephthalate – PBT

Polybutylene terephthalate or PBT, is a thermoplastic engineering polymer. PBT is second most important commercial polymer. Depending on the cooling rate and the moulding process, it comes in amorphous or semi crystalline microscopic structure. Furthermore, PBT has very attractive mechanical properties like high strength and hardness, good abrasive and heat resistance and great dimensional stability especially when fiber reinforced. Good combination of mechanical properties makes PBT one of the most desirable materials for design purposes [6],[5].

Mechanical properties of pure PBT are shown in Table 1.

Table 1. Mechanical properties of PBT [7]

| Mechanical property | Value |
|----------------------------|------------------------|
| Tensile modulus | 2800 MPa |
| Yield stress | 60 MPa |
| Yield strain | ~ 9% |
| Melting temperature | 225°C |
| Density | 1310 kg/m ³ |

Besides its pure state, PBT comes with reinforcements. Usually reinforcements are fiber like-materials like glass or carbon fibers in different percentages. Short (0.2 – 0.4 mm) or a long fibers (>1 mm) are routinely added in order to enhance mechanical properties but also to reduce probability of warpage [8]. Influence of different percentages of short fibers on mechanical response of PBT polymeric composite is given in Figure 1. Data from at a different fiber rates can be found in [7].

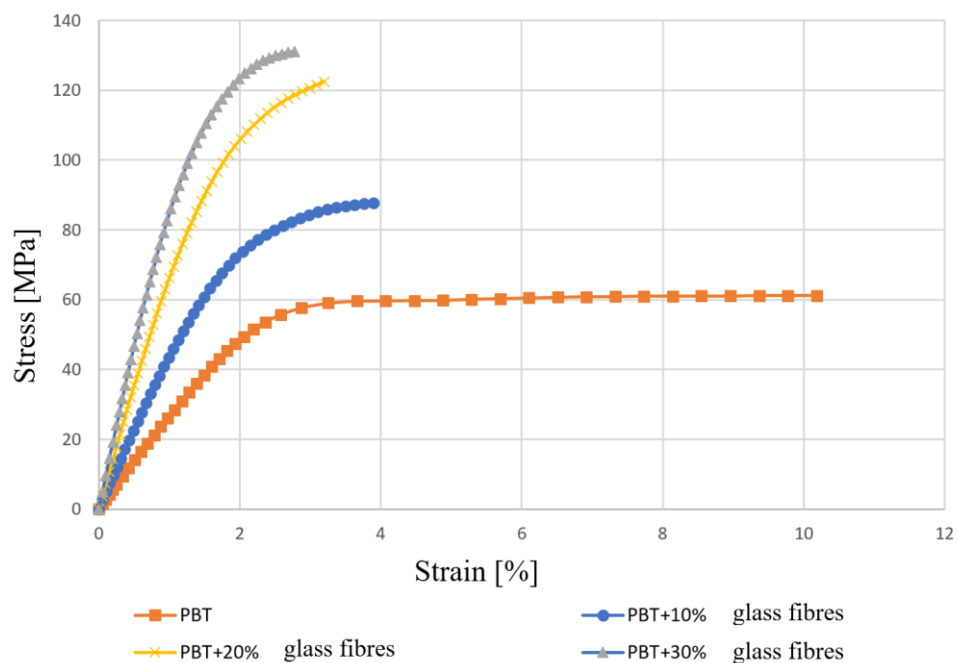


Figure 1. Influence of increasing short glass fiber share on mechanical response of polymeric (PBT) composite [9]

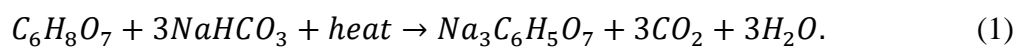
Seeing that the geometry of an experimental sample is very regular, change of injection moulding parameters, like temperature, injection speed and humidity, it's not possible to create holes inside of experimental sample. In order to validate numerical results, it's necessary to initiate growth of these holes inside of the sample. To make it work, in polymer mixture chemical compound is added. This compound under the influence of heat creates air bubbles. In following chapter chemical rule of creating air bubbles is shortly described.

2.2. *Hydrocerol*

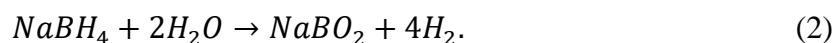
Hydrocerol[®] is trademark for chemical foaming agent. This compound is used for creation of foam-like components during injection moulding or extrusion with polymeric materials. During a material heating, chemical ingredients react under the heat and create the gases that are used for forming little bubbles of air inside of materials itself [10].

The primary purpose of this kind of chemical agents is to create form-like polymer constructions, whereby mass of component is reduced while mechanical properties stay the same or degrade slightly [11].

Hydrocerol[®] consists of sodium borohydride (NaBH_4) and the sodium bicarbonate/citric acid (NaHCO_3) / ($\text{C}_6\text{H}_8\text{O}_7$) mix which are encapsulated into pellets. The pellets of this chemical blowing agent are then fed into injection moulding machine along with polymeric material pellets. Sodium bicarbonate under the influence of heat energy from the mixture reacts with the citric acid to create water as follows:



From the other side, sodium borohydride reacts with the water from a result of previous reaction to produce hydrogen gas as:



As a byproduct of previous two reactions gases are created in melted material to create air bubbles. Usually *Hydrocerol* percentage in mixture is around 0,8 do 2% [12].

Using this kind of chemical agents, it's possible to create air bubbles in a regular geometry, like test samples, in order to imitate trapped air bubbles during injection moulding of real components.

2.3. Injection moulding

Injection moulding technology becomes known in industry since 1964. when French scientist Michael Gringras published patent in which describes principles of new technology. It did not take long for the industry to accept significant contribution of new technology for easier and quicker moulding of polymer components [13]. Today, injection moulding is one of the most important when effectuating technologies and it's not surprising that almost 90% of car components is manufactured using injection moulding [14].

Injection moulding is most used manufacturing technology for polymer components [15]. It includes melted polymer under high pressure that is injected into mold in shape of final product. Inside of a mold the melted polymer is cooled and it gets final shape. Usually spoken injection moulding is quick cycle process which enables production of huge quantities of components in very short time with great repeatability and dimensional accuracy [9].

In different ways, the stored polymer granules are fed into injector. Material is fed through shaft into melting cylinder. The melting cylinder does double function: he softens the material and injects it into heated mould. Depending on the used material, adequate pressure for injection moulding goes from 275 to 1100 bars and melting temperature between 150 and 425 °C. When mould is filled with material, cooling begins together with shrinkage which depends on material itself. Therefore, it's necessary to add additional material in the mould in order to avoid component shrinkage [9], [16], [17].

Irregularities that are formed during injection moulding are usually referred to irregularities inside of the component, i.e. volume irregularities. These latter irregularities, not visible to human eye, have significant influence on mechanical behaviour of a component. In order to avoid these problems, design advices and rules are given to minimise impact on expected mechanical response. Some of the most important rules are given in Figure 2.

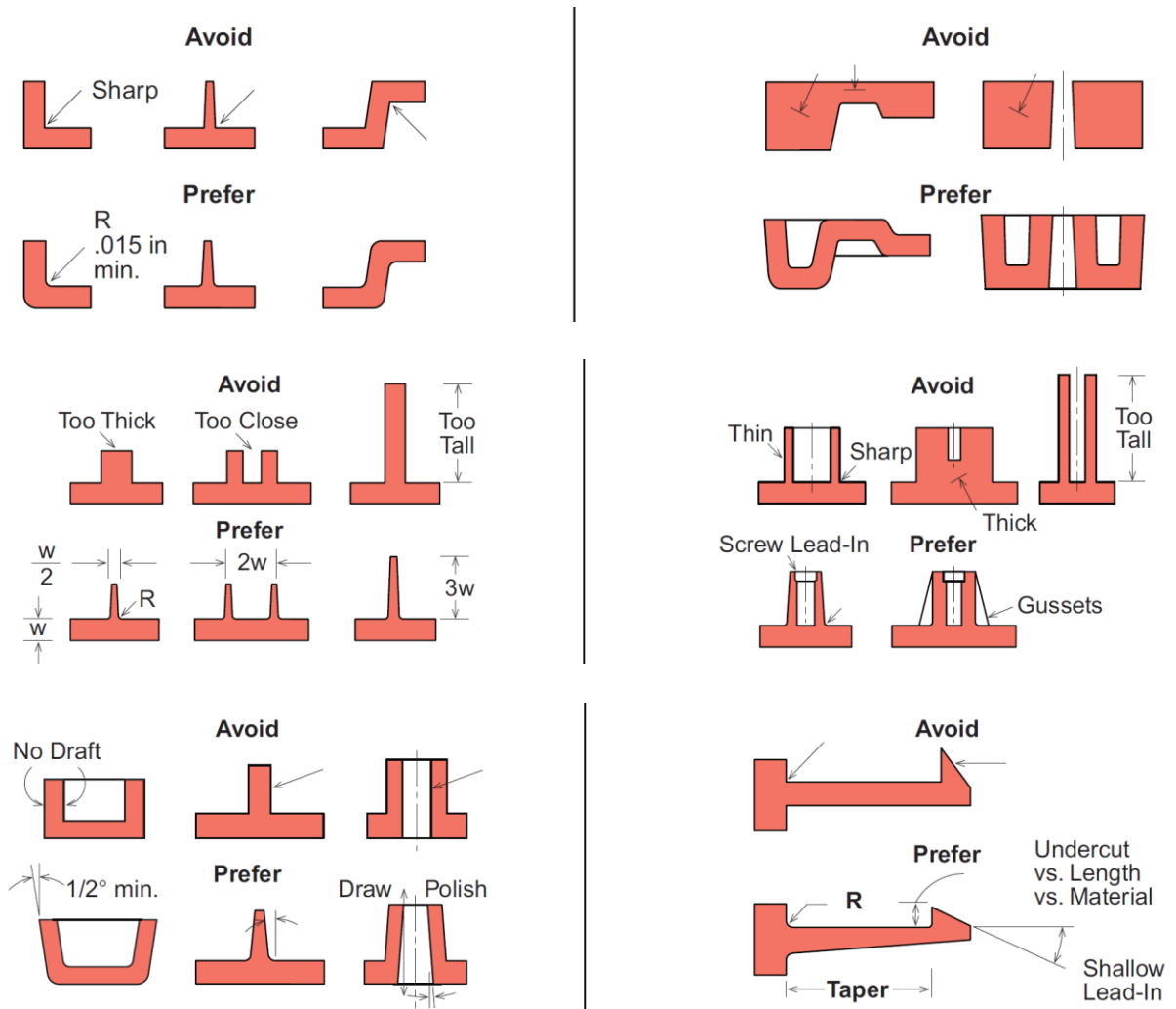


Figure 2. Injection moulding design rules and advices [9]

Except mentioned design parameters, other manufacturing parameters have big impact on irregularity forming. Parameters like melting temperature, mould temperature, cooling rate and pressure have influence on manufacturing process. Figure 3. shows shape of pore and its location on component.

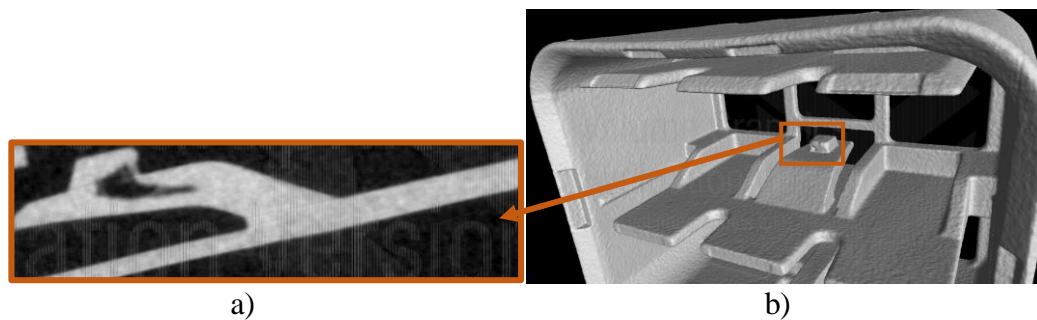


Figure 3. Irregularity on injection moulded component gained by CT, a) 2D section view, b) location on component

Very often the NDT methods are used to spot the irregularities that are located underneath the visible surface of component. Using NDT methods, it's possible to analyze variation of different technology parameters on irregularities that are occurred during injection process. Besides that, using FEM analysis, it's possible to determine at what level of irregularities component can withstand selected loading. Among other NDT technologies computerized tomography has huge advantage because it enables creation of accurate 3D model, usually, in form of point cloud. In following chapters, the physical principle of computerized tomography is explained.

2.4. Computed tomography

Computed tomography (mostly known as CT) is computer aided technology which uses ionizing radiation in order to create three-dimensional, outer and inner representation of a scanned object [18]. But what is tomography? The word tomography comes from the Greek words *tomos* – slice or section and *graphos* – to write, describe, or creating object sections in order to show interior of a scanned object [19].

Although CT technology is primary connected to medical application, during 1980s a huge potential of CT technology in the industry is revealed in the area of nondestructive testing, or NDT, but applying much greater energies then in medicine [20]. Computerized tomography in automotive industry is mostly used in quality control check of the parts that are casted or injection molded. Since very often these kind of components are regarded as safety components, it's important to understand and know mechanical behavior of parts that are not ideal [21].

After all, CT technology is still novelty in industry, especially in the way that is used to conduct this research. Because of that, theoretical background of CT technology is given in the following chapters.

2.4.1. Historical overview of computed tomography

At the end of 19th century, 1895th to be exact, the well-known German physicist Wilhelm Conrad Röntgen discovers the X-rays. Although Röntgen was awarded with

Noble prize in 1901 the full potential and application of X-rays are neglected up until 1972. [20]. That year British electronic engineer *sir* Godfrey Newbold Hounsfield designs first CT device which enters medical application in the same year [20], [22]. CT resounded strongly in medical diagnostics and is considered as one of the most important inventions after X-ray discovery.

But it's going to take a while before industry except computed tomography as an extraordinary tool for NDT. In mid 90s industry start to accept quantitative 3D analysis with simple volumetric and dimensional analysis. The development of stable radiation sources and more precise detectors CT is faced with fast growing development of devices that are capable of providing resolution at micro and nanolevel [4], [20]. With this kind of resolutions, a whole new range of application in industry is provided, for example composite material characterization, analysis of local density alteration and metrology.

Today, CT technology is applicable and these branches of industry:

- **Medical diagnostics** – Research of anatomy and oncology. Lower amounts of energy of ionizing radiation is typical,
- **NDT** – Metrology and quality control,
- **New material science** – Research of new composite materials, understanding of mechanical and material properties

CT systems for material analysis and industrial CT scanners are fundamentally different then their medical siblings. In industrial application our project is rotated in front of X Ray source, while at the clinical application object (usually a person) is fixed and the X Ray source and the detectors circles around object. That's why, by shifting the rotary gantry closer to X Ray source, sharper images are possible but with resolution sacrifice. For this reason, industrial application of CT scanners is much more flexible than clinical one. Because of the fact that in most cases, object is not sensitive to ionizing radiation, energy of radiation source can be higher in industrial application. By doing so, higher resolution and better quality off an image can be achieved [4].

2.4.2. Physical basics of CT technology

Essentially, every CT device, no matter where it is applied, consists of 4 main parts: a) X Ray source, b) Rotary gantry, c) detector and d) central processing unit [20].

X Rays are part of electromagnetic spectrum with wavelength smaller than 10nm. According to equation, smaller wavelength corresponds to higher energy, i.e. the energy of each photon, E , is proportional to its frequency, f .

$$E = h \cdot f = \frac{hc}{\lambda},$$

where h is Planck constant, c is speed of light, and λ is a wavelength of X-rays [20].

X Rays are generated by accelerating a beam of electrons and colliding that beam with a metal object (usually an anode). Electrons injected from the cathode surface are accelerated towards the anode. When electrons impinge on the target they interact with these atoms and transfer their kinetic energy to the anode. With this interaction, the result is a conversion of kinetic energy into thermal energy and electromagnetic energy in the form of X Rays. There are two ways of X-ray generation: *bremsstrahlung* and characteristic radiation. *Bremsstrahlung* radiation occurs when electrons pass very close to the nuclei of metal atoms but do not actually collide with any part of it. During this process, the electron is captured by the attractive force of the nuclei, where positively charged nuclei attract negatively charged electrons. The result is energy loss because of their interactions, which leads to photon emission with the same energy. The probability of this kind of irradiation is higher with a metal target as the atomic number increases. On the other side, characteristic radiation occurs when incoming electrons collide directly with one of the shell electrons, creating an electron vacancy. When this vacancy is filled with an electron from an outer shell, a discrete spectrum of X Rays is estimated. Nevertheless, this kind of radiation depends on the atomic number of the metal target and is characteristic because of the energy spikes that are superimposed on *bremsstrahlung* radiation. When properly maintained, an X Ray tube is working, approximately 1% of the energy generated is emitted as X Ray. The rest of the energy is converted to heat, so the anode, inside of a vacuum tube, has to be cooled [23]. Focal point presents one of the most important characteristics of industrial CT scanners. Depending on the size of a focal point, industrial CT scanners can be divided into macro,

micro and nano systems. Macro CT scanner is used for large objects while micro and nano scanners are used for small objects where accuracy and resolution are more important than size of a scanning area. Besides the focal point, the shape of a beam has important meaning. In modern city scanners cone beam is used. Nano CT scanner uses X Ray from a focal point that is smaller than $1\ \mu\text{m}$, while micro CT uses focal point from $1 - 50\ \mu\text{m}$. Depending on the measuring range and the resolution, CT scanners are divided into groups according to Figure 4.

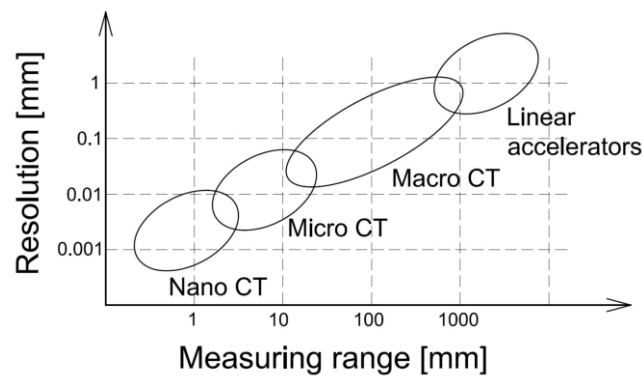


Figure 4. Types of CT scanners according to size of a focal point depending on resolution and measuring range [20]

The detector is used for measuring attenuation of an X Ray as beam passes through an object. Key role of the detector is transformation of an X Ray into electrical signal. There are different kinds of detectors, but lately flat panels are the most common. They provide direct transformation of ionizing radiation into electrical signal [20].

The rotary gantry stands in between an X Ray source and the detector on which an object is placed. During rotation, different 2D sections or slices of an object are recorded. When object is scanned from different angles, a 3D representation of the model is reconstructed [20].

2.4.3. Image reconstruction

At the end of acquisition process, reconstruction algorithms are used for forming the 3D representation of the scanned object. The reconstructed volume consists of voxels. *Voxel* is primitive element of 3D structure and it's the smallest element of volume mesh that can be individually discern (Figure 5.). A voxel is analogue version of a pixel in 3D [20], [24].

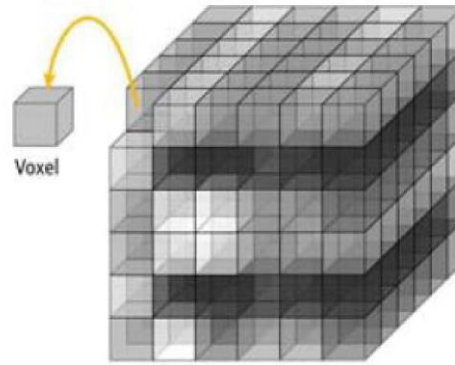


Figure 5. Voxel as a part of reconstructed volume [20]

Projection is an image that is generated inside of a detector when an X Ray beam is send through an object. These projections are generated all around object by gantry rotation. In order to show the image reconstruction process simple 2D case is considered (fan-beam planar X-ray).

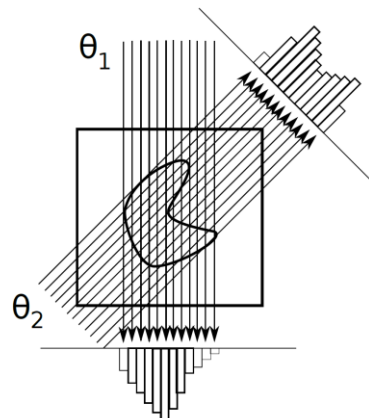


Figure 6. Principle of 2D planar X Ray beam. attenuation of an X Ray which passes through an object is measured on 1D detector for two different angles θ_1 i θ_2 [19]

Absorption is physical property on which CT technology is based on. The mechanism that allows image reconstruction is called attenuation of X Ray beam. The attenuation is quantified by, so called, a linear attenuation coefficient μ which varies with the location inside the object. The physics that describes this mechanism is called Lambert-Beer law of attenuation [19].

Let the incident extra intensity is denoted by I_0 . For the X Ray beam which passes through homogeneous block of length D with constant linear attenuation coefficient, the outcome intensity of X Ray beam is:

$$I = I_0 e^{-\mu_0 D}. \quad (1)$$

In more interesting material where attenuation coefficient depends on position x or $\mu(x)$, the outcome intensity of X Ray beam is:

$$I = I_0 \exp\left[-\int_L \mu(x) dx\right]. \quad (2)$$

The intensity I , in the preceding expressions, is called transmission while the corresponding quantity

$$b = -\log\left(\frac{I}{I_0}\right) \quad (3)$$

it's called absorption.

The origin of become a graphic image reconstruction is usually referred do the paper *Über die Bestimmung von Funktionen durch ihre Integralwerte längs gewisser Mannigfaltigkeiten* written by Johanna Radon from 1917. Among other things it is proved that is possible to reconstruct the object from a full set of line integrals over all.

The general expression of Radon transform is:

$$p_\theta(s) = \int_{L_{\theta,s}} f(x, y) dl, \quad (4)$$

where $\theta \in [0^\circ, 360^\circ]$ i $s \in [-1, 1]$.

The Radon transform is described as *forward problem* or how (ideal) X-ray projection data arise in a parallel beam geometry. But if we want to reconstruct image from measure data the invert Radon transform is used or so called filtered back projection (FBP) which states:

$$f(x, y) = \int_0^\pi q_\theta(x \cos\theta + y \sin\theta) d\theta. \quad (5)$$

FBP is very often used in practice. But right away the question arises, how many projections or angles is necessary to create image reconstruction of scanned object? For that it's necessary to find compromise between quality of reconstructed image and speed of imagery constructions and data quantity by transforming continuous function into a discrete one. Figure 7 shows the quality convergence of reconstructed image.

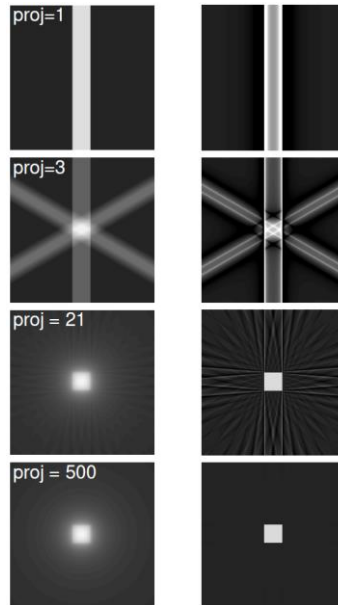


Figure 7. Number of projections influence onto quality of reconstructed image. with big amount of projections FBP is very efficient [19]

Another significant parameter in the image reconstruction is *threshold* value. *Threshold* transforms grey value into binary value. The result is image that consists of two sets: one presents the background (usually the value of 0 or gray value of air) and the other one is material (object). The *threshold* defines the border between object and background while created surface, while scanning 3D object, is joined to the object itself. Figure 8 shows example of surface determination using threshold value (the green line in 2D case) between voxels (pixels in 2D case) with the different HU or grey value.

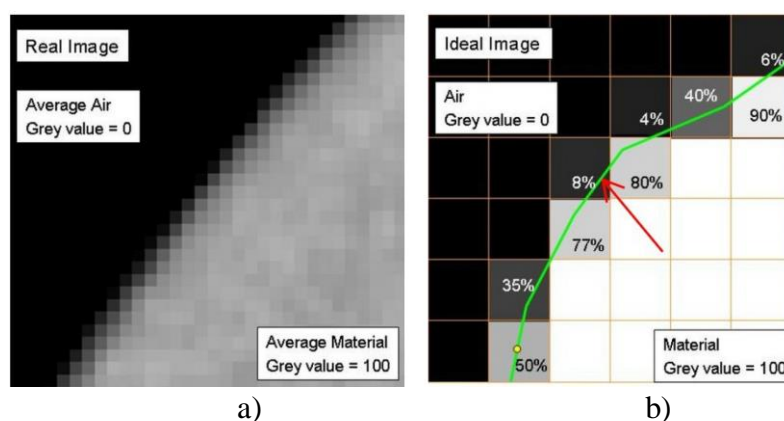


Figure 8.. Example of surface determination using threshold value, a) real image, b) ideal image [20]

The impact of *threshold* value determination is presented in Figure 9. The value varies in a certain range while the cylinder part diameter is measured.

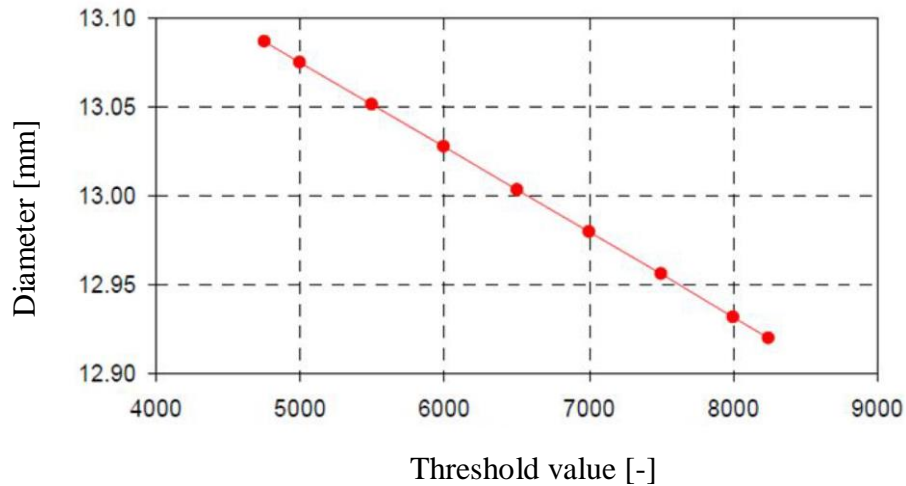


Figure 9.. Variation in diameter measurements of a cylindrical part for different threshold values. The diameter is calculated using an ideal cylindrical surface to the resulting CT point cloud. [20]

Unlike metrology which requires resolution of voxels greater than the size of the porosities, for irregularity detection resolution of voxel can be smaller than volumetric unit. To achieve that, it's necessary to have efficient contrast in combination with partial volume effect. The latter effect it's occurred when voxel is divided into two sections which represents two different materials. In this case, both materials contribute to grey value of single voxel [25]. This effect is particularly significant when scanning heterogeneous materials, like fiber reinforced polymer that are mentioned above. Fiber reinforced polymers are widely used when designing lightweight components [4], [26].

3. Mechanical behaviour of investigated materials

3.1. Direct numerical simulation

The term direct numerical simulation or DNS refers to very detailed numerical analysis without having to use multiscale simulation and homogenization procedures or defining Representative Volume Element (RVE). Using DNS material microstructure is explicitly modeled using different techniques like computerized tomography, synchrotron etc. Respectively, DNS method is process of modeling and analyzing whole heterogeneous material microstructure without any simplification or homogenization.

Encouraged by the astounding growth in computing power, DNS method, over the last two decades was faced with huge progress. Computers combined best aspects of mechanical models and ability to process vast amounts of data and therefore are exceptional tools for testing complex nature of materials and often providing new insights of mechanical behaviors of composite materials [27], [28]. Besides mechanical behavior analysis, over the years many efforts an attention was given to predict material constants of fiber reinforced composites through the combination of material constants of its constituents. It is physically meaningful since fiber composites are not chemical compound but physical mixtures. Under this point of view, several mixture models have been proposed like classic mixture rule (Voight – Ross model). Advances in computer hardware and parallel computing have now made possible engineering analysis of a large-scale microscopic models that are directly discretized with 3D finite elements with DOFs that extend level of more than tens of millions [29].

The current numerical analysis can be grouped into following two approaches:

- Macroscopic - the composite materials are assumed to be continuum with homogenized material properties based on isotropic, orthotropic or anisotropic constitutive equations. With this approach global behavior of composite structure is predicted in an "average sense". However, this approach has limitations in describing the local behavior. Consequently, this approach cannot give accurate evaluation of local stress and prediction of failure.
- Microscopic - the composite materials are regarded as mixtures of different materials that are isotropic or anisotropic where different constituents are modeled separately. The biggest advantage of this approach is detailed and local information about constituents, their behavior and interaction. One of the most used microscopic approaches is using unit cell and representative volume element. Basically, the unit cell method that reduces the size of the problem to one unit cell with periodic boundary conditions. But it should be noted that this microscopic approach is another methodology of homogenization since it says it assumes identical state in periodic distribution of the cells [27], [28].

In the DNS approach the whole composite structure is directly modeled through separate modeling of fiber and matrix at the microscopic level [28]. Very often for example a full microscopic modeling is necessary for understanding and prediction of failure mechanism since the failure of composite material is initiated from microscopic level and propagated through macroscopic level [27].

As aforementioned, microscopic model can be obtained using simple CAD modeling of whole specimen for layered composite or fiber-reinforced composites with aligned fibers. But when using composites with random fiber distribution the best way for obtaining DNS model is using radiographic imaging techniques like CT or synchrotron. The latter models contain very detailed information about microscopic structure and defects inside the specimen.

For the purpose of this research, 3D X-ray micro-Computed tomography is used for obtaining DNS models. After that, grey value threshold is applied to separate voids from the matrix. Since voids have been made of gas (CO₂...) they have low density and very

low value of HU, in comparison with PBT. Histogram is used to show contribution of each grey value inside of scanned object. One of histograms of scanned object is shown in Figure 10.

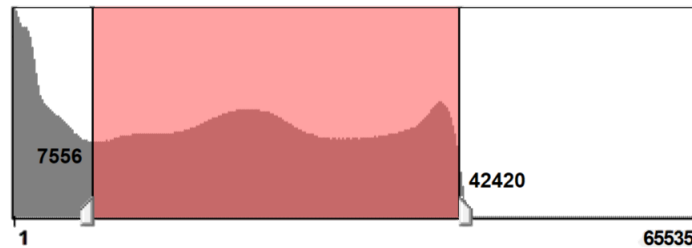


Figure 10. Typical histogram of scanned testing probe

In this way, using threshold value voids are excluded from main material. Bigger lower threshold value is applied in order to show voids more clearly, since accuracy of voids and sample itself is not so important and does not contribute to final mechanical properties.

For purposes of obtaining the DNS model, several software were used. After image acquisition, data were introduced to VGStudio software. Since CT, that was used in this research, has *.rek* format, it's necessary to transform *.rek* file to DICOM image stack. DICOM (Digital Imaging and Communications in Medicine) is standard format in medical imaging but it's widely used in industry. After that, image stack is imported in MIMICS software, where threshold value is applied, and 3D model is created. Current 3D model is just point cloud and it's necessary to create volume mesh. To do so, model is imported in 3Matic, which is MIMICSs extension. Finally, after meshing in 3Matic, input file for Abaqus is created and imported to Abaqus where boundary conditions and loads are applied, and analysis is conducted.

3.2. Mechanics of heterogeneous materials [30]

Polymer under uniaxial tension exhibits nonlinear behavior as soon as stress (σ_{xx}) exceeds yield stress or, σ_Y (Figure 11). If the stress/strain response is independent of the strain rate, then this material can be modeled using elasto-plasticity theory.

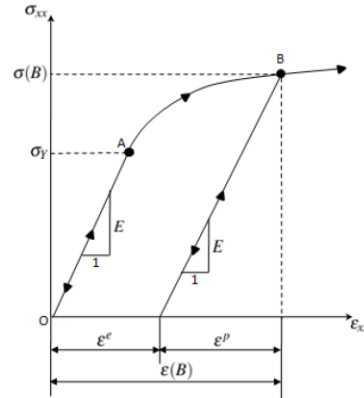


Figure 11. Idealized stress/strain curve of a polymer under uniaxial tension in x-direction

For purposes of this research, J2 plasticity model is used. J2 is elasto-plastic constitutive model defined as:

$$\sigma_{eq} = \sqrt{J_2(\boldsymbol{\sigma})} = \left(\frac{3}{2} \mathbf{s} : \mathbf{s}\right)^{\frac{1}{2}}, \quad (5)$$

where J2 is second invariant of the deviatoric stress tensor \mathbf{s} , and it is expressed as:

$$J_2 = \frac{3}{2} (\mathbf{s} : \mathbf{s}), \quad (6)$$

$$J_2 = \frac{3}{2} \left[\boldsymbol{\sigma} - \frac{1}{3} Tr(\boldsymbol{\sigma}) \mathbf{I} \right] : \left[\boldsymbol{\sigma} - \frac{1}{3} Tr(\boldsymbol{\sigma}) \mathbf{I} \right], \quad (7)$$

$$J_2 = \frac{1}{2} [(\sigma_{11} - \sigma_{22})^2 + (\sigma_{22} - \sigma_{33})^2 + (\sigma_{33} - \sigma_{11})^2 + 3(\sigma_{12}^2 + \sigma_{23}^2 + \sigma_{31}^2)]. \quad (8)$$

For uniaxial loadings, the von Mises equivalent stress is equal to axial stress.

In G2 constitutive model, response is assumed to be linear elastic as long as equivalent stress is lower than initial yield stress. The Cauchy stress and the elastic strain are then related by:

$$\boldsymbol{\sigma} = \mathbf{C} : \boldsymbol{\varepsilon}^e, \quad (9)$$

where \mathbf{C} is Hooke's operator. When σ exceeds the initial yield stress, the response becomes nonlinear and plastic deformation appears. In this case, the Cauchy stress is given by:

$$\sigma = \sigma_Y + R(p), \quad (10)$$

where $R(p)$ is hardening stress and p is the accumulated plastic strain, expressed as:

$$p(t) = \int_0^t \dot{p}(\tau) d\tau, \quad (11)$$

with,

$$\dot{p} = \frac{2}{3} \sqrt{J_2(\dot{\varepsilon}^p)} = \sqrt{\frac{2}{3} (\dot{\varepsilon}^p : \dot{\varepsilon}^p)}. \quad (12)$$

For uniaxial loadings, the accumulated plastic strain is equal to the axial plastic strain. The 2/3 factor enables to account for transversal shrinkage due to incompressibility of plastic strains.

4. Experimental testing

In the beginning of experimental research, standard ISO testing samples are created using injection moulding, with dimensions defined by ISO 527 (Figure 12).

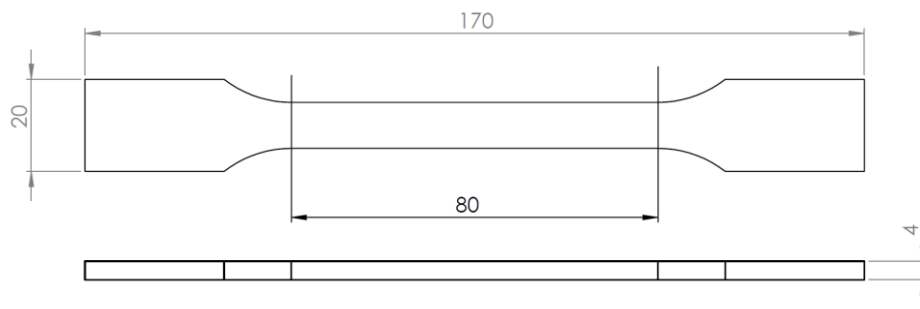


Figure 12. Dimensions of standard ISO 527 testing sample

The measuring part of testing sample is 80mm, and the wide sections on each end of testing sample are for grip on testing machine. Before testing, samples were scanned under micro X Ray computed tomography. From there on, samples are tested using uniaxial test machine. Obtained results are then compared with numerically analysed samples.

4.1. Hydrocerol impact to mechanical properties

As everyone would assume, there is impact on macroscopic properties of parts that are combined along with *hydrocerol* chemical blowing agent. Because of the initial purposes of this kind of chemical agent in injection moulding parts, latter parts have slightly lower density with bigger volume. The change of density in testing samples is visible on CT scan (Figure 13).

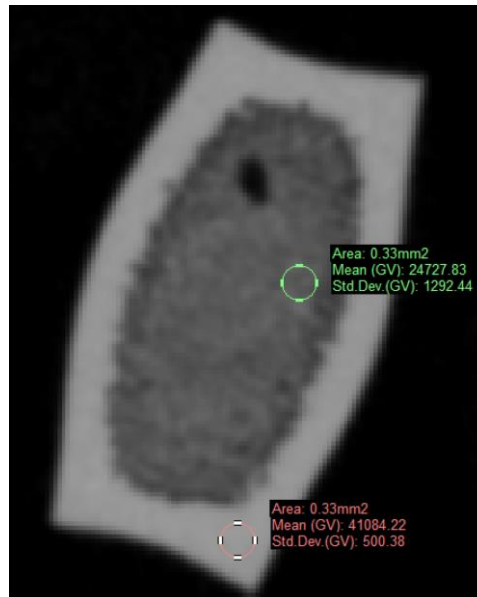


Figure 13. CT slice of testing sample. Change of density under influence of hydrocerol chemical blowing agent is visible in form of greyvalue variation

Higher value of density directly corresponds to higher value of HU or greyvalue. On CT data or slices, higher value of greyvalue are presented in form of brighter pixels (or voxels in 3D) and vice versa. This means that brighter pixels have higher density or higher linear attenuation coefficient.

Density deviation on testing samples cross section can give us hint on how hydrocerol works inside polymer components. Lower density in middle part of sample (Figure 13) implies that expansion of polymer resin starts from inside. Because of the expansion, melted polymer is pressed against mould walls and has higher density (Figure 13 shows that greyvalue in the middle part of the cross section it's a half of the greyvalue of external parts).

The testing sample in Figure 13 is manufactured like other injection moulding parts with one change. After injection in mould and before hardening inside mould, mould is opened in order to hydrocerol expand in melted polymer. Because of this, cross section is not rectangular.

All the testing samples are experimentally tested on unidirectional test machine (Figure 14). The strain rate in experiment was 20 mm/min. With this strain rate, it can be said that experiment was quasistatic.



Figure 14. The testing setup: the testing machine and the experimental sample positioned respectively

With all this said, the influence of *hydrocerol* adding is investigated. Four different samples were created with difference in manufacturing technique. Description of manufacturing techniques were described in Table 2.

Table 2. Sample groups and manufacturing description

| <i>Group name</i> | <i>Manufacturing description</i> |
|--------------------------|--|
| Normal PBT sample | Pure PBT sample injection moulded without any adding |
| 1% open mould | Injection moulded PBT sample with 1% of Hydrocerol adding. After injection moulding process, mould is opened in order give space for material expansion. |
| Not dried | Injection moulded sample. PBT material were previously moisturized with water. |
| 1% closed mould | Injection moulded PBT sample with 1% of Hydrocerol adding. After injection moulding process, mould is left closed and sample is cooled inside the mould. |

Results from experimental uniaxial testing of presented groups, along with reference curve obtained from manufacturer [7], are shown in Figure 15.

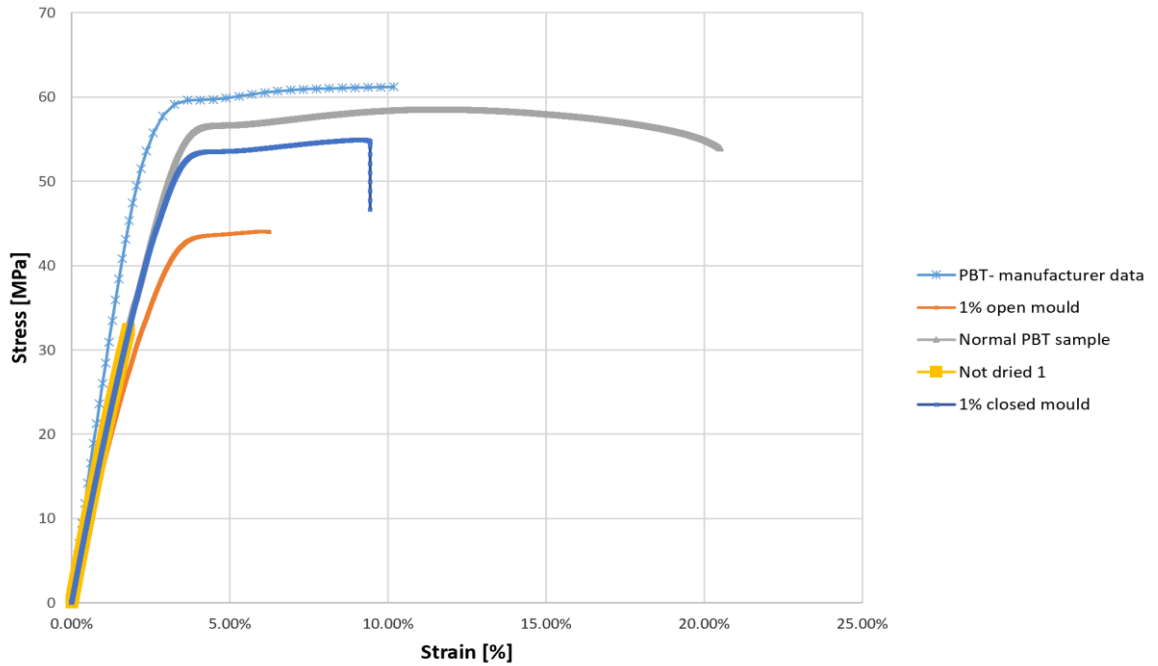


Figure 15. Results from four groups of experimental samples with different manufacturing techniques

When the test was carried on the unreinforced PBT testing samples, the glass fibre reinforced testing samples are also experimentally tested. The Figure 16 shows the unidirectional results from 20% glass reinforced PBT sample

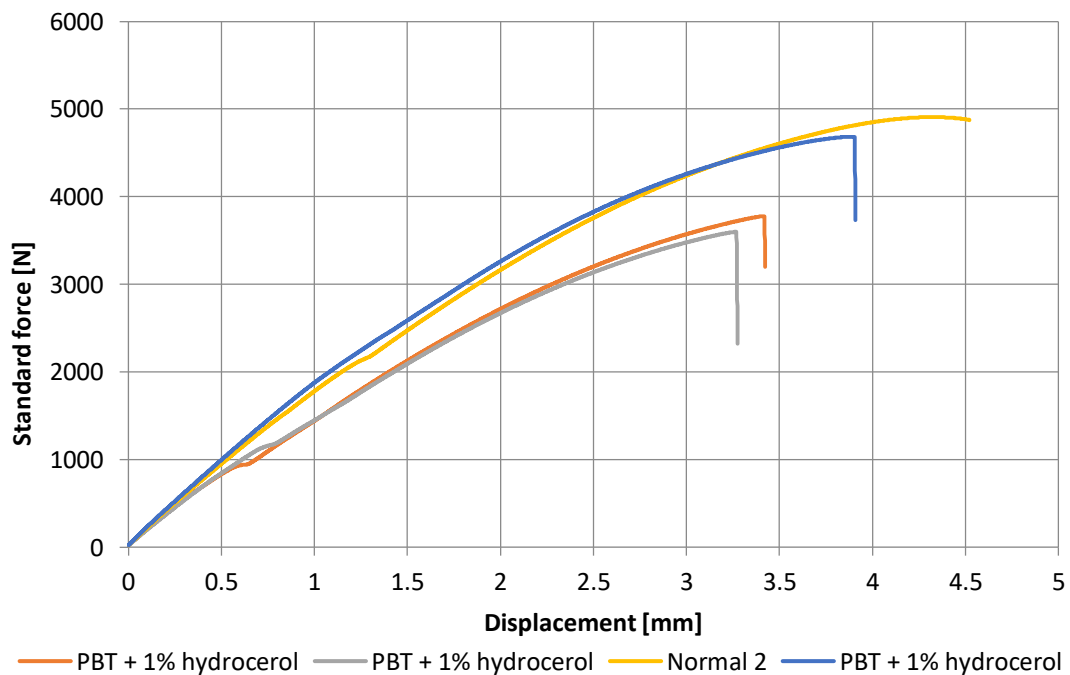


Figure 16. Experimental results for different PBT samples with hydrocerol additive in comparison with pure PBT sample. Significant deviation in results is visible for samples

5. Numerical testing

In the beginning of the experimental research, numerical analysis was conducted on ideal models in order to validate numerical results. Except results, models are used to see impact of representative volume element (RVE) size to results shift.

In first group of models, a set of seven different RVE sizes are modelled. Models are containing irregularities in form of pores (voids). In this set of models, 2% of random placed pores are included with size of 0,5 mm. The set of models is shown in Figure 17.

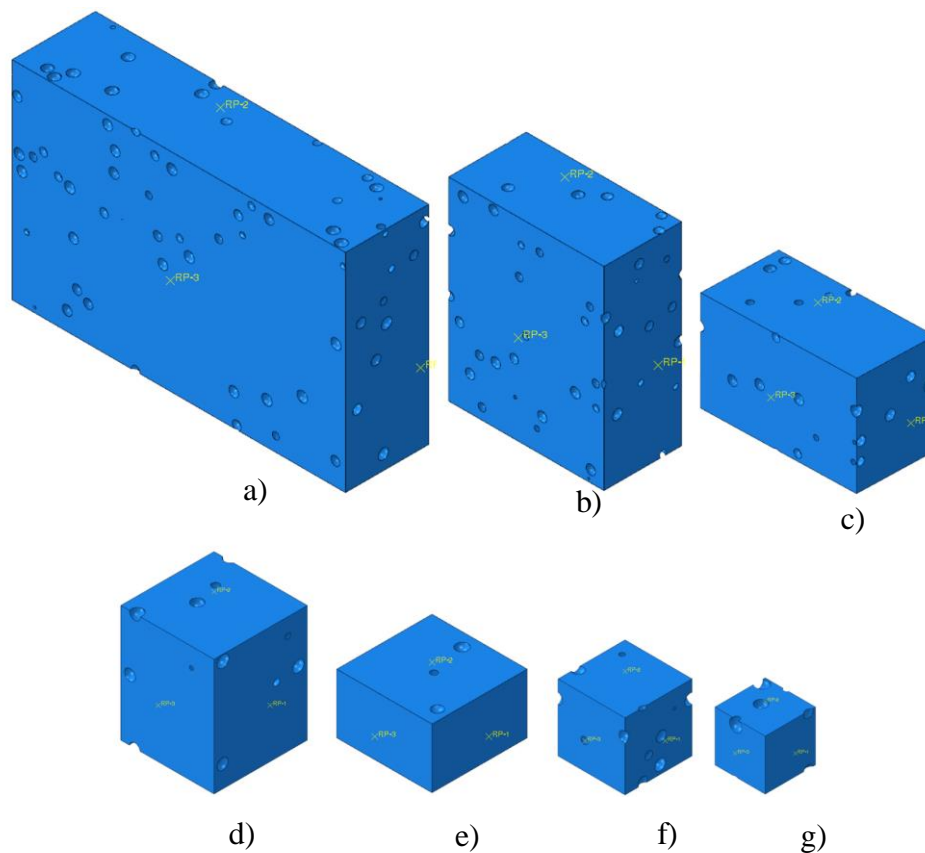


Figure 17. Set of models with irregularities in form of pores. Models contain 2% of randomly placed pores with size of 500nm

Also, the model size and the number of finite elements (FEs) are shown in Table 3.

Table 3. Model size and number of FEs for different unreinforced RVE models

| <i>Model size</i> | <i>Number of FEs</i> |
|-------------------|----------------------|
| 16x10x4 mm | 462 795 |
| 8x10x4 mm | 210 287 |
| 8x5x4 mm | 106 254 |
| 4x5x4 mm | 77 647 |
| 4x2,5x4 mm | 39 535 |
| 3x3x3 mm | 38 697 |
| 2x2x2 mm | 23 513 |

The results from previous set of models (Figure 18) with comparison with non-porous experimental test shows that there is very little impact on mechanical properties. Respectively, size of RVE also does not give impact on mechanical properties.

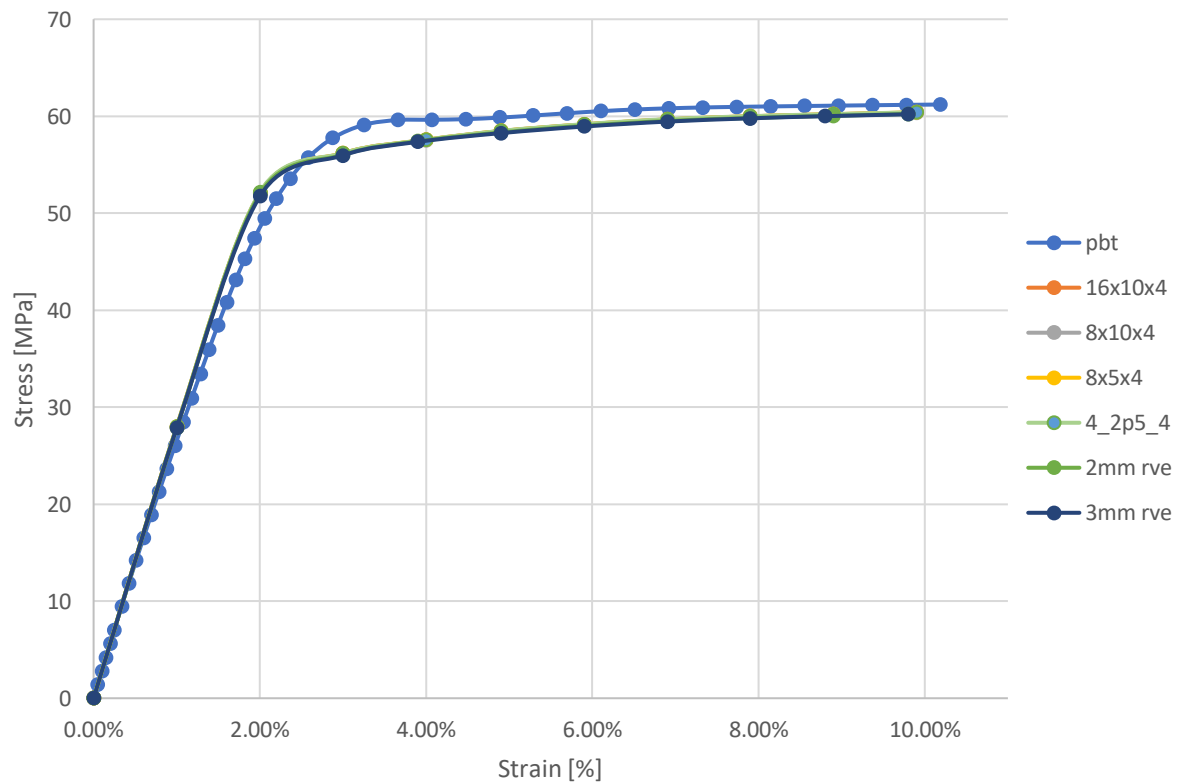


Figure 18. Result comparison with different size RVEs

After the test was carried out on unreinforced models, fibre reinforced models are simulated numerically. Two groups of models are analysed. The first one is with unidirectional placement and the other is with random placement of the fibres. Again, for the purposes of this research different RVE size models are used (Figure 19).

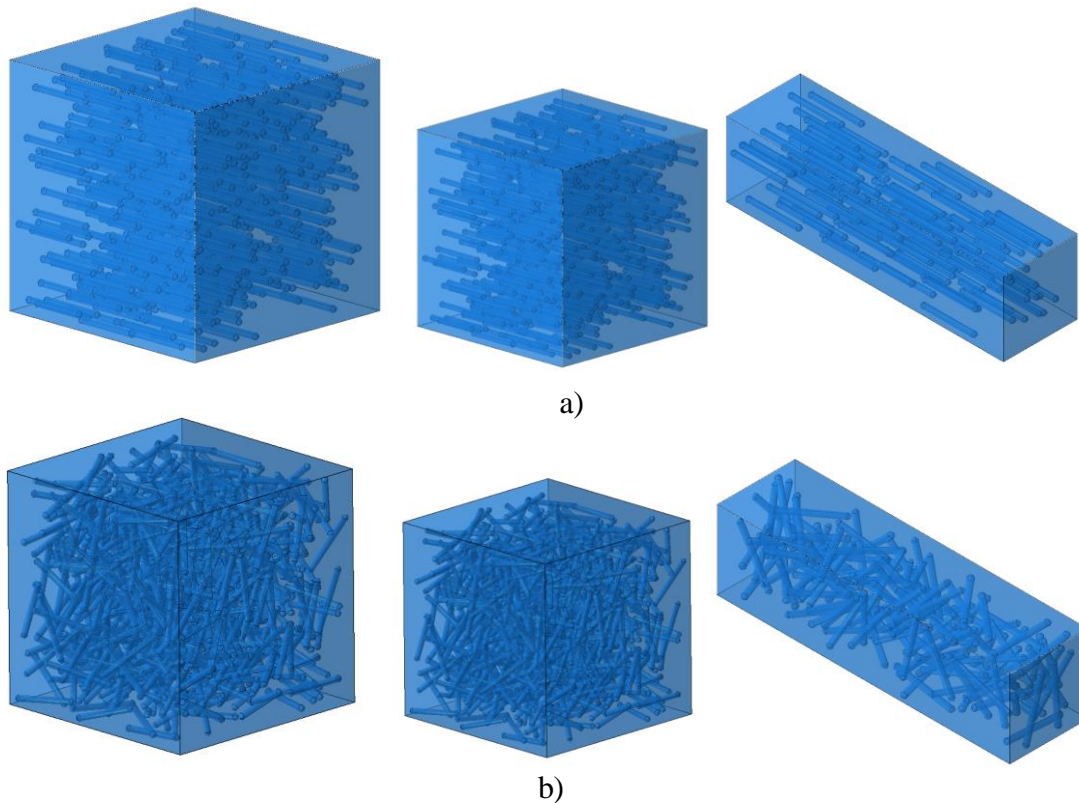


Figure 19. Different RVE size models. RVE model groups with: a) unidirectional fibre placement and b) random placement.

Also, the model size and the number of FEs for each RVE model is shown in Table 4.

Table 4. Model size and number of FEs for different fibre reinforced RVE models

| Model name | Model size | Fibre number | FEs number |
|-----------------------------|-------------------|---------------------|-------------------|
| <i>Unidirectional group</i> | | | |
| U0.3 | 0,3x0,3x0,3 mm | 121 | 240 738 |
| U0.4 | 0,4x0,4x0,4 mm | 287 | 5 876 706 |
| U0.75 | 0,75x0,1x0,1 mm | 135 | 268 510 |
| <i>Random group</i> | | | |
| R0.3 | 0,3x0,3x0,3 mm | 115 | 297 632 |
| R0.4 | 0,4x0,4x0,4 mm | 264 | 6 254 312 |
| R0.75 | 0,75x0,1x0,1 mm | 135 | 273 710 |

The results from different RVE sizes for the random placement are given in Figure 20a and for the unidirectional placement in Figure 20b.

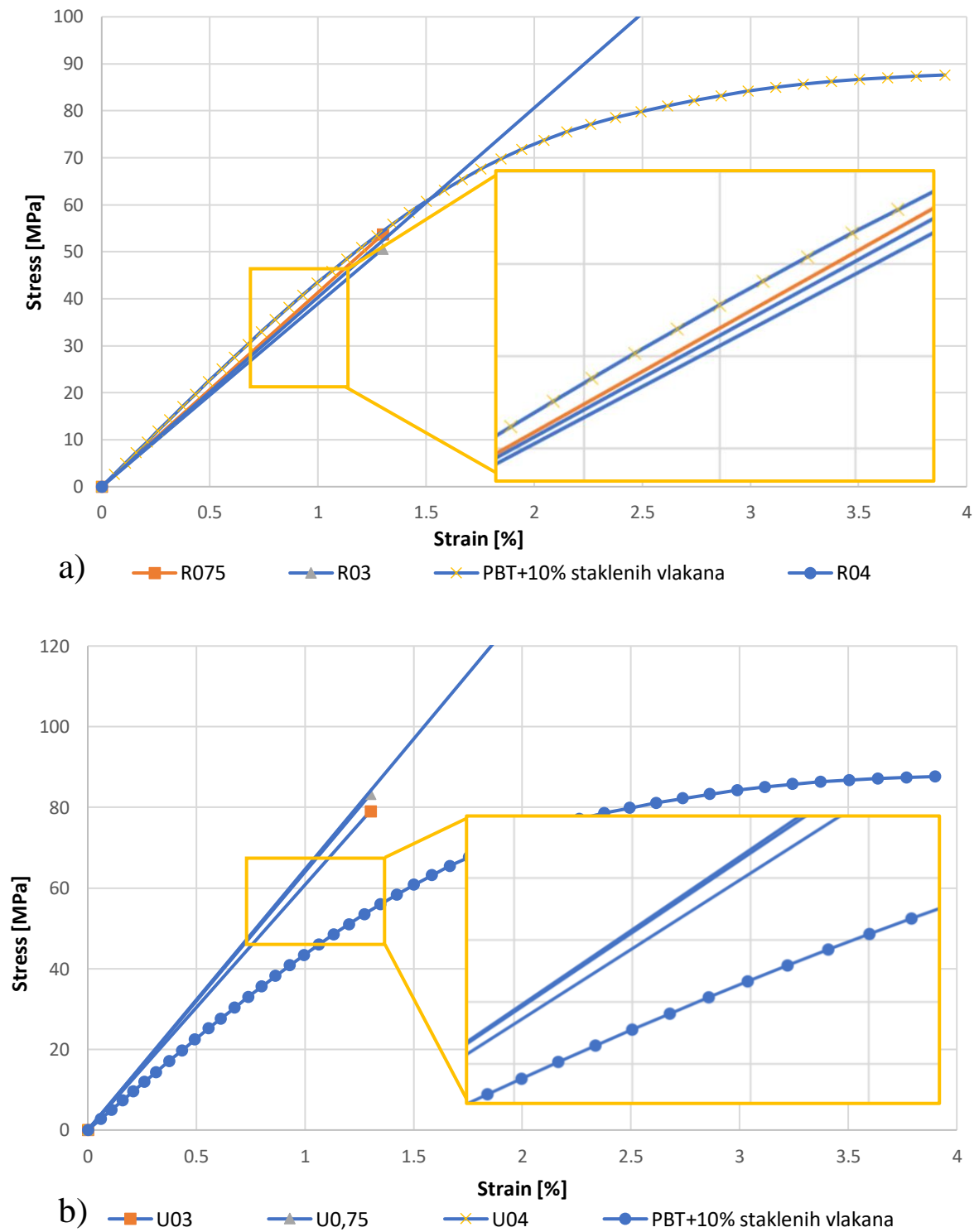


Figure 20. Comparison results from DNS analysis for different RVE size models from: a) unidirectional RVE group, b) random RVE group

5.1. CT models

After the analysis was conducted on referent set of models, the other set of models is now used. This time, models are obtained with micro X-ray computed tomography (CT models). Because of the thing that pores influence was primary objective of this thesis; CT models are used in form that only real geometry of sample is exported. Density deviation in testing samples, described above, is not applied on volume finite elements.

Models are reduced from single specimen. This specimen is manufactured with injection moulding and imperfections were created with *Hydrocerol* chemical agent, described above. From this sample 3D model (Figure 21) is created using Mimics software.

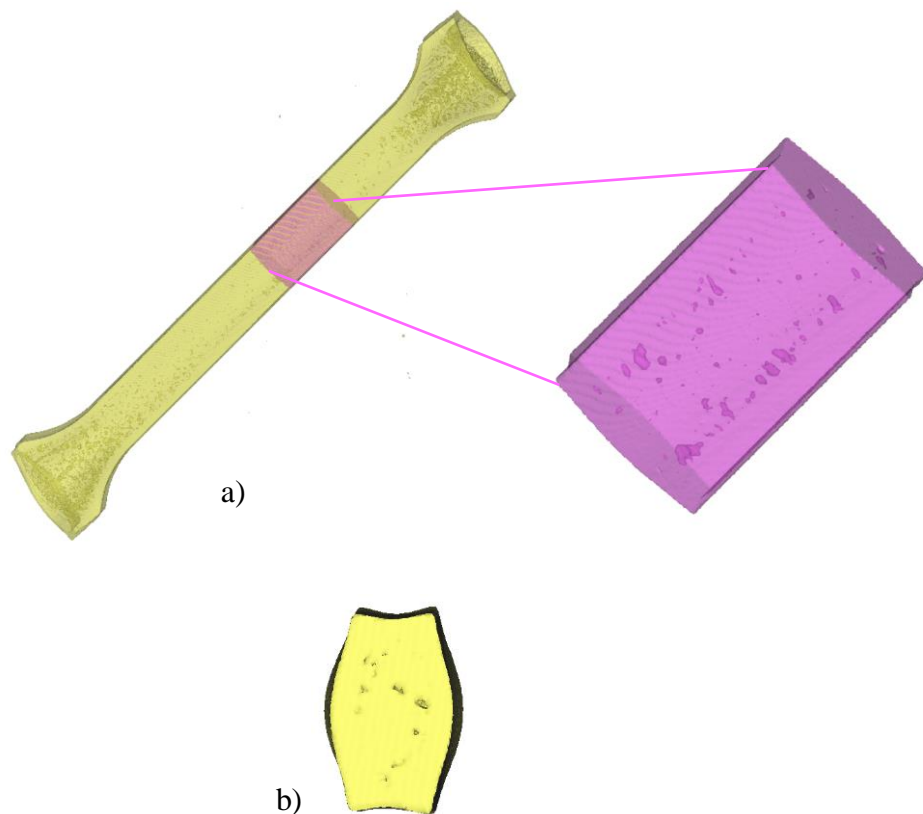


Figure 21. a) 3D model of experimental sample obtained by CT scan, b) cross section of scanned sample

Also, from the Figure 21 it's visible that sample is porous. Since model is obtained with high accuracy, it contains a very big amount of data stored in form of point cloud. Figure 21b shows that, in comparison with the ISO standard model (Figure 12), the

sample has irregular cross section. That is the result of *Hydrocerol* which "inflates" the material from inside – out.

Regarding latter, one fifth of measuring part of sample, which is 16mm in length, is cut from sample in order to minimise data generation (Figure 22a). Different sizes of RVE are separated from this model, respectively. Sizes of each RVE model is listed in (Table 5) with dimensions and number of elements required to create volumetric mesh. These smaller models are separated as one half of previous model.

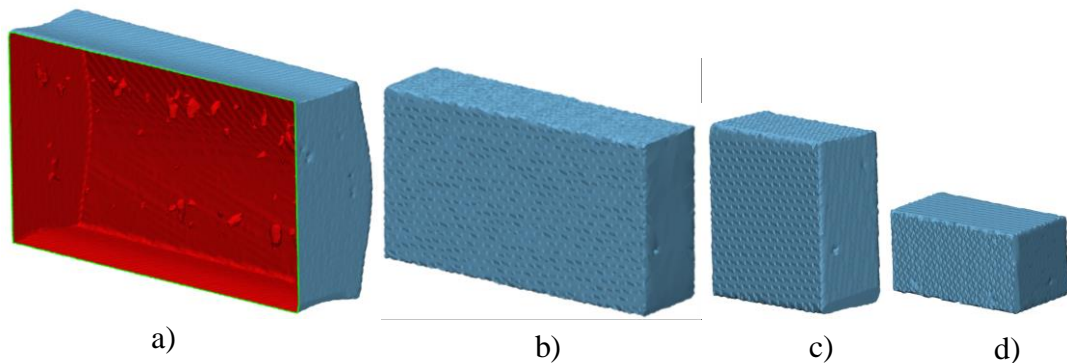


Figure 22. a) Cross section of full model with voids, b) large model, c) medium model, d) small model

During RVE modelling, Mimics file is imported to 3Matic extension. There, very small voids (smaller than $0,005\text{mm}^3$) are considered as noise and deleted in order to improve mesh quality. Also, to reduce number of elements and to reduce local stress concentration *smoothing* feature is applied. With this feature, surface triangles are reduced to form curve. Comparison before and after *smoothing* feature is shown in Figure 23.

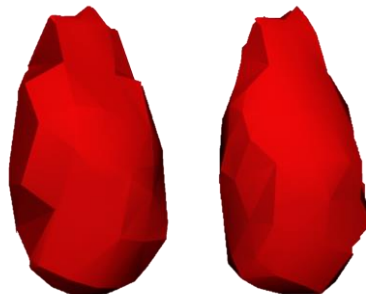


Figure 23. Void inside the volume, a) before smoothing feature, b) after smoothing feature

The volumes of the voids are in range from 0.005 to 0.388 mm³ (Figure 22). In 3Matic, automatic volume mesh generation is not possible. Considering the inclusion, it is necessary to have holes in volume mesh. This is feasible to model only with *split-manifold* feature, which creates base model as subtraction from volume inclusions.

Because of the way how *Hydrocerol* works, by expanding the material with CO₂ bubbles, the geometry of experimental sample is not regular. The cross section is not rectangular as it would be if there were not *Hydrocerol* chemical adding.

Table 5. Different size of RVE models from CT scan with information of elements and voids number

| <i>Name</i> | <i>Size [mm]</i> | <i>Number of elements</i> | <i>Number of voids</i> |
|------------------|--------------------------|---------------------------|------------------------|
| Full model (1/5) | 16.69 x (~5) x (~9.6) mm | 2 282 424 | 50 |
| Large model | 16 x 9.3 x 4 mm | 1 030 917 | 39 |
| Medium model | 7.8 x 9.3 x 4 mm | 845 838 | 9 |
| Small model | 7.8 x 5 x 4 mm | 471 245 | 7 |

All models are meshed with tetrahedral quadratic elements with C3D10 label. Afterwards, models are imported to Abaqus software, where boundary conditions are applied to models (Figure 24.). Boundary conditions on the two edges are introduced to avoid rotation and rigid body motion.

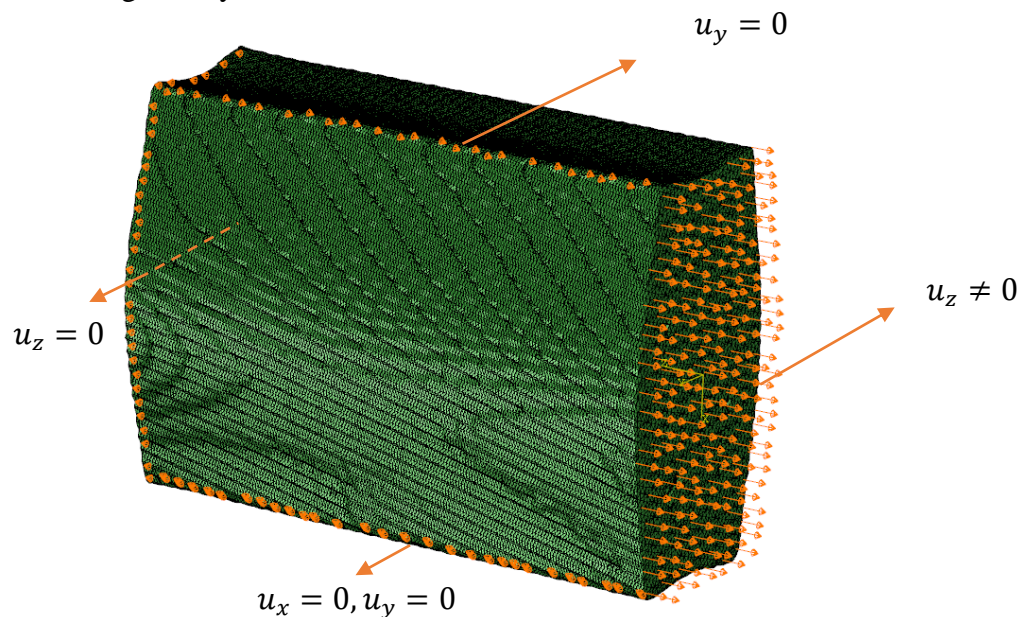


Figure 24. Boundary conditions applied on models

After analysing mentioned CT DNS models with different RVE size, the results are compared with the experimental ones. The comparison diagram is shown in Figure 25.

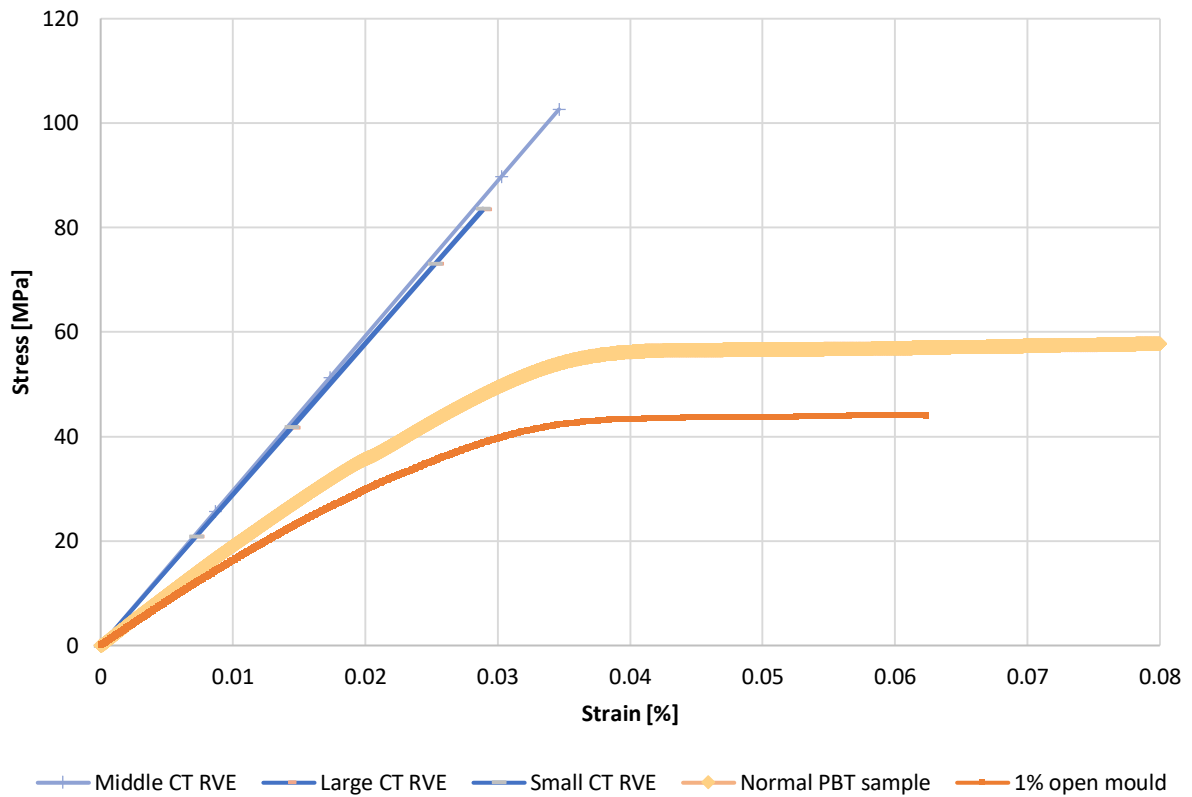


Figure 25. Comparison between different sizes RVEs and experimental test

6. Mechanical response of the connector housing

After validation of numerical results with experimental test on testing samples, research is conducted on real components. One of housings with irregularities is taken for research. Figure 26 shows connector housing with its connector positioning assurance (or CPA). CPA's key feature is to additionally secure the connection of wires inside the connector.

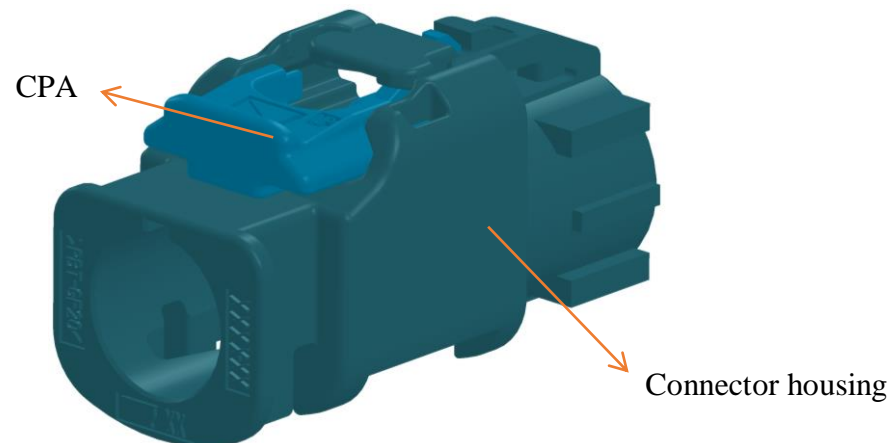


Figure 26. Yazaki connector housing with appropriate connector positioning assurance

Because of the fact that critical section in shown assembly is located on the CPA, numerical and experimental investigation is conducted on CPA.

During CPA installation in connector housing, CPA is loaded with displacement on secure locking as shown in the Figure 27 along with critical section.

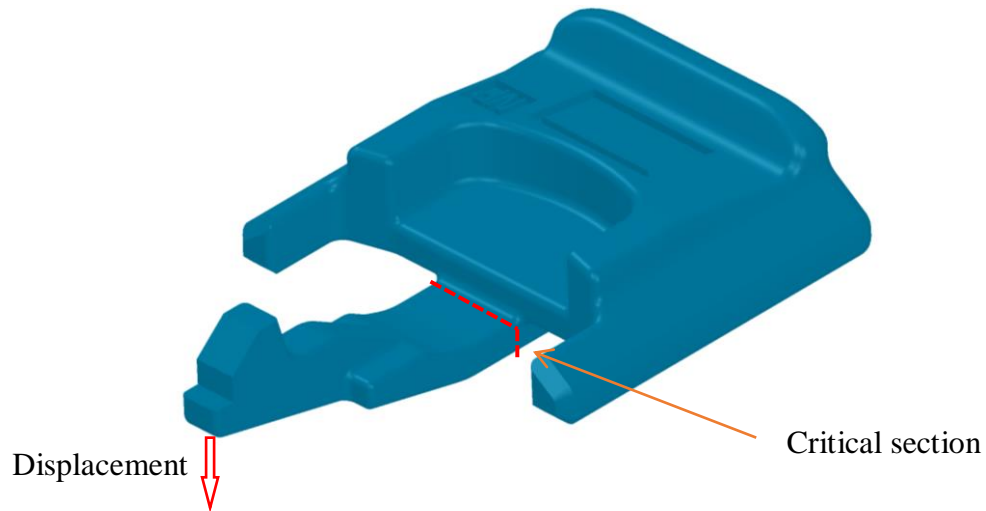


Figure 27. Connector positioning assurance (CPA) of the connector housing

6.1. Experimental testing of CPA

Experimental tests are conducted on CPA. The specimen used in experimental testing does not contain any irregularities (at least not ones in form of pores). The specimen is tested to compare and validate numerical results. The testing is conducted on flat table, where strength of CPA locking is investigated. Figure 28 shows experimental setup where CPA is tested.



Figure 28. Experimental setup where connectors CPA is tested

Experiment is conducted with lever where displacement is applied onto CPA's locking. The force and the displacement are measured on the device itself and force – displacement diagram is plotted. Figure 29 shows results from experimental test. The sudden rise of force after 1.1 mm displacement happens when locking gets in the contact with the table. The point when the rise occurs is important, because numerical simulations are guided by this point.

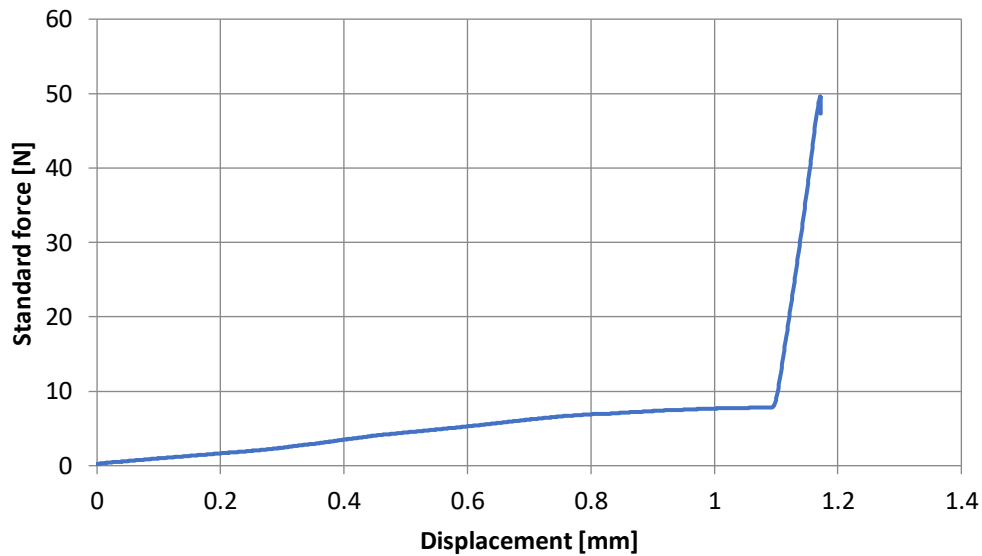


Figure 29. Experimental results of CPA

6.2. Numerical results of the CPA

After experimental test, numerical analysis is set like the experimental one so both results are mutually comparable. The DNS model is obtained using micro X-ray computed tomography. In order to lower the number of finite elements, only ROI is selected for analysis. The rest of the CPA is for easier handling and the neglected area will not have major influence on numerical results.

The CT obtained DNS models of selected ROI of CPA is shown in Figure 30. Also, appropriate boundary conditions and loading are applied on the model. During analysis, non-linear formulation (*nlgeom*) of FE is turned on, because the displacement is significant, and small displacement theory cannot describe the mechanical behaviour of analysed component.

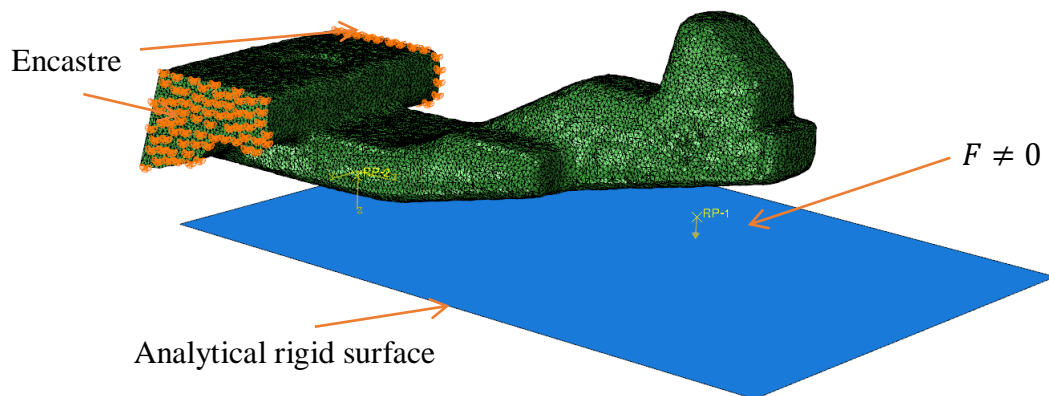


Figure 30. The CT DNS model of an ROI of housing CPA with boundary conditions and loading

The contact between CPA and the table in experiment (Figure 28) in numerical analysis is simulated through rigid surface. Also, surface to surface contact between CPA itself and the rigid surface is added.

The deformed shape of the ROI is shown in Figure 31. This model does not contain any porosities and since, experimental analysis was conducted on this very own part, numerical results are validated.

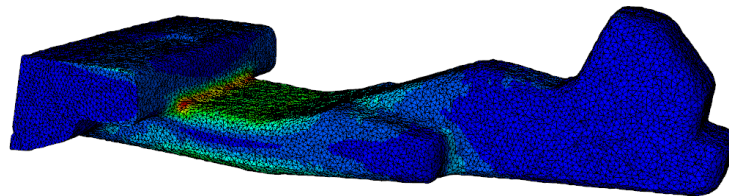


Figure 31. Deformed shape of the ROI of investigated CPA

Numerical results in comparison with the experimental ones are shown in Figure 32.

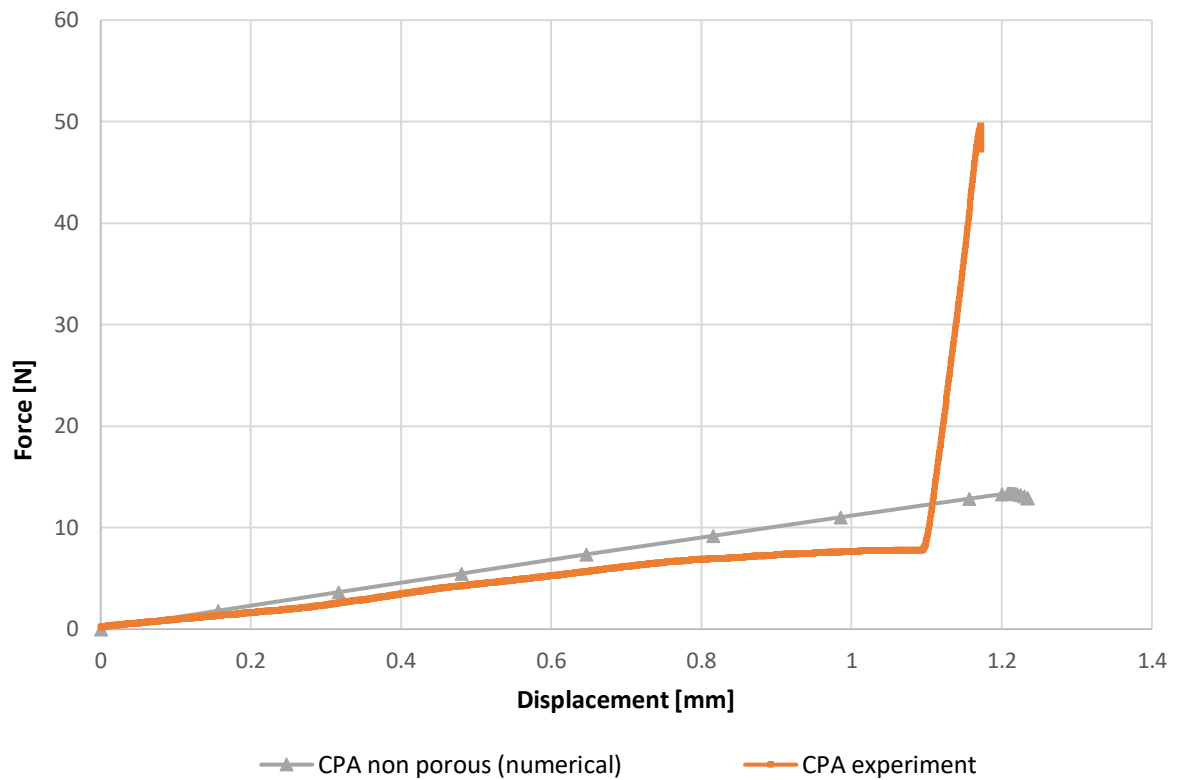


Figure 32. Comparison results between CPA experimental test and the DNS of the ROI based on CT scans

During the initial research programme, plan was to investigate the influence of different percentages of porosities on connector mechanical behaviour. In this plan, DNS models would be obtained with micro X-ray CT scanning. Since CT technology in industry is still novelty, a lot of technical issues appeared and only one CT scan was satisfactory, the porosities must be added thought software. The scan of the selected CPA had very few porosities.

In order to investigate porosities influence, CT slices are processed to create different percentages of porosities. Using Mimics software, slices in all three directions are modified. Deleting the pixels in dozens of slices, it's possible to create pores in 3D model with different sizes and shapes (Figure 33).

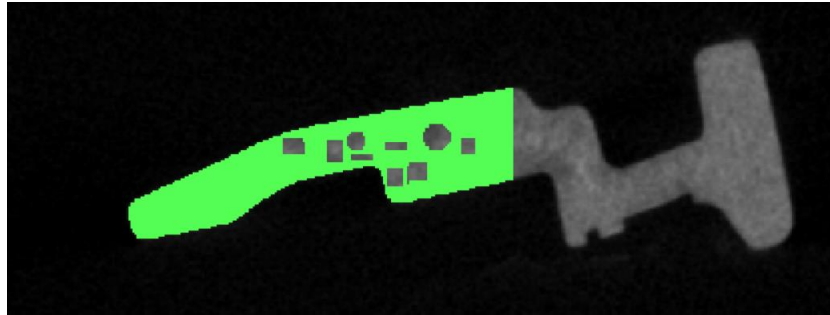


Figure 33. CPA slice. Deleting the pixels in slice in order to create pores

Three situations are investigated. DNS models have 3 different percentages of porosity's as shown in Table 6.

Table 6. DNS models with different porosities

| <i>Model name</i> | <i>Porosity volume percentage</i> | <i>Number of porosities</i> | <i>FEs number</i> |
|-------------------|-----------------------------------|-----------------------------|-------------------|
| First model | 0% | 0 | 316 526 |
| Second model | 1% | 10 | 196 152 |
| Third model | 2% | 17 | 209 439 |
| Fourth model | 3% | 25 | 241 653 |
| Fifth model | 5,5% | 41 | 344 838 |

Most of the porosities are located close to critical section, so volume percentage in critical section is greater than the one listed above. Transparent DNS model in Figure 34 displays the DNS model with 2% porosities.

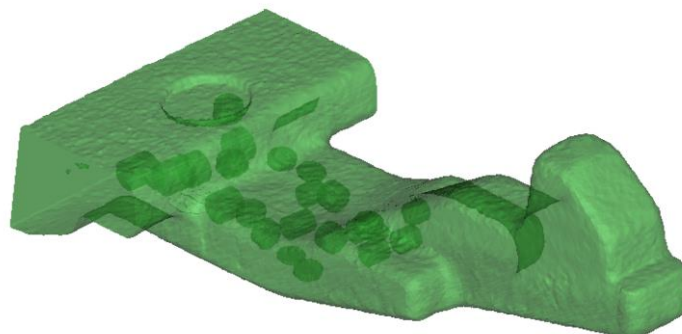


Figure 34. Porous DNS model. Porosities are located close to critical section

The results, carried on the modified CT models, with manually and randomly added pores, are given in Figure 35.

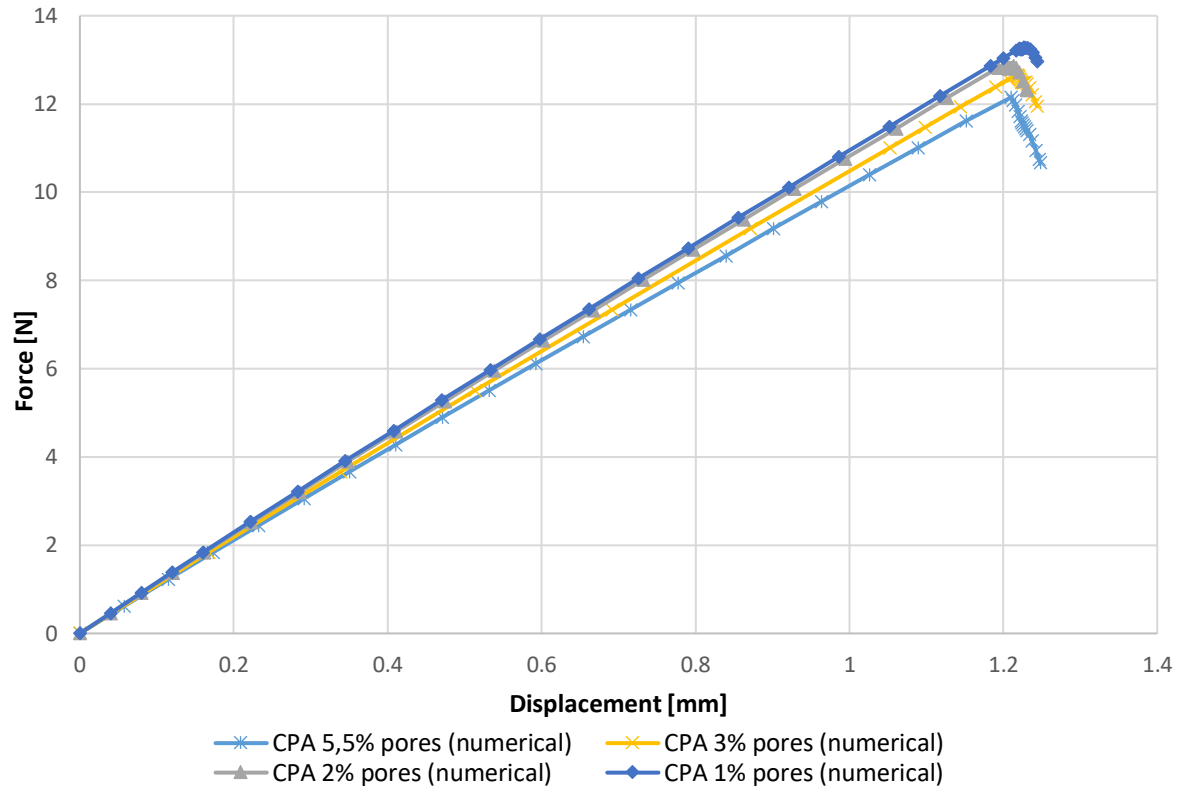


Figure 35. Comparison results for the different percentages of porosities in the critical section of the CPA component

Now, when all the experimental results are given and compared with numerical ones, the discussion is given below. The difference between the experimental and numerical results is explained and along with future improvements.

7. Discussion

In the first section of the thesis, theoretical background is given, where theory of CT technology, material properties and DNS method are described. After the theory of each section of research is given, experimental and numerical analysis were conducted and results from both are given in comparison.

In the beginning of the research, the main object was to investigate the influence of porosity on mechanical properties of component. But, before experiment and numerical simulations can be carried out on the real components, investigation of the influence must be carried on the testing samples. With this done, numerical results and procedure can be validated.

As described above, *Hydrocerol* additive is used to create pores inside the testing samples. Before additive was accepted as solution for pores, different manufacturing methods are used to create pores. Lowering or increasing parameters to the limit values, like material humidity, material and mould temperature, injection pressure etc. did not contribute to pore forming inside the testing sample. The main reason for this is that testing samples have very regular geometry (Figure 12) and material flow is unobstructed and very laminar. Because of this, additive is chosen as only way for pore forming.

Hydrocerol works on molecular level. Creating molecules of gas, it expands material by creating pores. Only sample from Table 2 that has visible pores is the one with open mould. So, tests were conducted on this type of samples. The bad thing about hydrocerol adding is that, because of the latter process, cross section of the sample is not rectangle.

As shown in Figure 15 it's visible that *Hydrocerol* impact is visible even than there are no pores visible. Like the sample with 1% of hydrocerol, where pores are not visible, strength and strain of the sample is lower than the normal injected sample without additive. Even though the sample is scanned under a micro X-ray CT, change in density is not visible and lower values of strength and strain can be attributed to the molecular chain damage.

Regarding the investigated sample with visible pores the strength is significantly lower than the normally injected PBT sample as expected mostly because of pore influence and because of the density change from *hydrocerol*.

But before the uniaxial tension test was carried out, porous sample was scanned under micro X-ray CT. From here, DNS model was created with different size of RVE's. Since, this kind of modelling, using the CT scan, is still novelty in industry, a lot of impediments were having to be solved.

DNS method is very straight-forward technique and in most cases DNS models are containing a lot of elements and DOF's, respectively. But DNS models from CT, have a whole new level of element number as can be seen in Table 5 where small RVE DNS model contains around half of million elements. Using even the high-end working station, manipulation and simulation of this kind of models is very demanding and time-consuming.

As it can be seen in Figure 25, results from DNS CT model has significantly greater strength than experiment even it has pores inside. This reason for this deviation, is cross section of the specimen. The area used for the stress calculation was the average rectangle rather than the real cross section. Another, more influential, parameter is material properties added to the FE. Since porosity is the investigated topic, density deviation from additive in the middle of the sample is not considered, and the material properties from PBT were added to FEs. When we consider all deviations from expected results, it can be said that numerical simulations of the different RVE sizes can describe the mechanical response and that numerical results are validate thought experimental testing.

As mentioned above, DNS CT models are demanding a lot of computing power. In order to avoid full scale, time-consuming models and simulation, RVE models are introduced. The RVE size influence is investigated on two types of models: academic, i.e. numerical models imported from software and CT model. As can be seen from Figure 18, there is no difference in mechanical behaviour when using software DNS models without fibre reinforcement. This allow us to use even the smallest model to simulate real mechanical behaviour of the testing sample. But in the contrast, when using RVE from software the deviation is visible and increases with a decrease of the RVE size. The reason why this happens on the fibre reinforced RVE models, is that fibres cannot fully fit in smaller RVEs. Since the fibre length is 150 microns, the smallest RVE must be larger than 0.2 mm. In addition, comparison results from Figure 20, shows that unidirectional models offer greater strength then the models with random fibres. The random placement of the fibres fits better the experimental results then the unidirectional placement, respectively.

Models gained by CT are also showing slight deviation (Figure 25). But, as can be seen, the difference between small and large model can be neglected when, considered computing time of small model is around six times shorter than the computing time for large model.

During preparation of the CT DNS models and the CPA component, Mimics software is used for 3D model creation. Since micro X-ray technology is very precise and the resolution is high, very small pores and defects on the surface are visible. To lover the number of DOF's and improve mesh quality, the different smoothing factors are applied to the surfaces and notably distorted elements. With this done, slight error is imbedded into DNS model. But considering the computing time and the mesh quality, the model inaccuracy can be neglected. And indeed, model can be considered even more accurate than the raw CT model to which noise is removed.

After numerical validation of PBT samples and fibre reinforced PBT, the experimental and numerical tests are carried on CPA. The comparison results from CPA

experimental and numerical tests (Figure 32) shows slightly greater strength of the numerical model than the experimental one.

Because of the technical issues during the CT scanning, the few scanned components do not contain pores. As mentioned above, using Mimics software and slices modification, pores are initiated inside the CPA. Since the validation of the numerical results of the CPA component is verified on the experimental test, we can predict that models with initiated pores will give satisfying results. As it can be seen in Figure 35, the strength of is decreased with the increase of the pore percentage. Even though this behaviour was anticipated, in the contrast, the strength cutback is lower than expected.

Since lots of technical issues came across, during the research, especially numerical part and CT model acquisition, many of the problems are resolved. Thing that weren't even considered as potential problems, created lots of difficulties during the research. Most of the problems were software based. Importing the models from CT with different file extension and conversion to the appropriate form took a lot of precious time. Since the CT models of the testing samples and the CPA scans were considerably big data files, and RVE size was investigated, abovementioned software was used. Even with this model reduction and ROI and RVE creation, the files significantly big are above average. Regarding the latter, the model preparation took more time than expected. Creation of the volume mesh, different RVE size modelling and numerical analysis itself had given us the conclusion that RVE size had to go down. Even when using professional workstations, with large number of processors and threads, simple manipulation and selection with this huge data amount is reduced. Estimated computing time for the analysed model was around four to five hours with additional time for the result analysis.

As described, this kind of DNS analysis is just minor part of the offers from CT technology, possibilities of today's computing power and numerical mechanics. Future CT DNS models will bring accuracy to a whole new level. Pore influence and other imperfections from injection moulding and other manufacturing technologies will be

investigated furthermore. As a result, components with imperfections, doesn't need to be considered as write-offs.

Regarding the simulation's accuracy, material assignment from CT can be taken. The density of the voxels can be directly transferred to corresponding FE. This means, that experimentally tested samples and numerical models have identical material properties. Results from the testing samples, where the density variation in cross section is significant, can be improved and more accurate.

8. CONCLUSION

In this thesis, the porosity influence is investigated on testing samples and real components. The numerical simulations are verified using appropriate experimental tests. Mechanical response of different size RVE's and the DNS model is investigated, respectively.

It is shown and described that numerical simulations can adequately describe behaviour of porous components. Difference in results from experiment and simulation are mostly user errors. Input data, like material assignment of the FEs and nonrectangular cross section are contributing to the overall error. Future improvements in this area, can substantially contribute to the accuracy.

The RVE size investigation, on academic DNS models and on CT based DNS models, shows that using even the smallest RVE size, numerical error is not significant, and the mechanical behaviour is satisfying. This means, that is not necessary to use full scale models with dozens of millions of elements, when good results can be achieved with smaller models. Overall computing time and data acquisition is much shorter which saves time and money. The opposite of what was expected, it is shown that testing samples have random placement of the fibres, rather than the unidirectional fibre placement which has significantly greater stiffness.

Using *hydrocerol* additive for pore initialization in testing samples, the mechanism of the additive is shown. Also, the change in density is visible on the CT scan. Regarding future of the testing samples with *hydrocerol*, it should be considered to change the way of initialization of the pores. Hydrocerol additive is not engineered for this kind of tests. Variation between different testing samples is significant. In some cases, the tensile modulus is even larger than normal PBT sample. The reason for this is the density which

is bigger in marginal part of the cross section (Figure 13) and it contributes to the overall strength of the sample.

Regarding the analysis on the connector component, numerical tests, based on CT DNS model, are also validated with appropriate experimental test. It was shown that CT based DNS model can describe mechanical behaviour. Since no porosities are founded inside the CPA volume, the pores are initiated on CT slices and corresponding 3D models. Different pore percentage is investigated and it is shown that, slight drop of strength up to 10% is visible between non-porous model and the model with 5,5% of pores.

At the end, to conclude, this research may not give a significant data but the technical issues and the overall problems that were resolved are of great importance for the future research. The micro X-ray technology for this kind of porosity influence is novelty but, as can be seen from the above described results, it can provide great insight for mechanical response of different components.

Since almost every injection moulded component has some kind of irregularity, this kind of simulations is and, hopefully, will become even more used, especially in industry. Growth of polymer component, especially in automotive industry is not stopping, at least not for now. Using CT technology is possible to see and understand the occurrence of these imperfections. With this knowledge, design practice can be improved in order to minimise the possibility of pore occurrence.

In addition, the components with irregularities can be inside threshold values of product specification, which means that even then, manufactured parts can be used. This saves time and money, with good ecological footprint.

BIBLIGRAPHY

- [1] V. Phongsathorn, “No Title,” 2019. [Online]. Available: <https://www.quora.com/Which-are-the-worlds-biggest-industries-in-dollars>.
- [2] J. Holbery and D. Houston, “<art-3A10.1007-2Fs11837-006-0234-2.pdf>,” no. November, 2006.
- [3] W. Elmaraghy, H. Elmaraghy, T. Tomiyama, and L. Monostori, “Complexity in engineering design and manufacturing,” *CIRP Ann. - Manuf. Technol.*, vol. 61, no. 2, pp. 793–814, 2012.
- [4] L. De Chiffre, S. Carmignato, J. P. Kruth, R. Schmitt, and A. Weckenmann, “Industrial applications of computed tomography,” *CIRP Ann. - Manuf. Technol.*, vol. 63, no. 2, pp. 655–677, 2014.
- [5] T. Filetin, F. Kovačiček, and J. Indof, *Svojstva i primjena materijala*. Zagreb: Udžbenici Sveučilišta u Zagrebu, Fakultet strojsarstva i brodogradnje, 2013.
- [6] Polymerdatabase.com, “PBT @ polymerdatabase.com,” 2018. [Online]. Available: [http://polymerdatabase.com/Polymer Brands/PBT.html](http://polymerdatabase.com/Polymer%20Brands/PBT.html).
- [7] P. B. Pbt, “CAMPUS ® Datasheet,” pp. 1–4.
- [8] H. C. Tseng, R. Y. Chang, and C. H. Hsu, “Numerical prediction of fiber orientation and mechanical performance for short/long glass and carbon fiber-reinforced composites,” *Compos. Sci. Technol.*, vol. 144, pp. 51–56, 2017.
- [9] L. Corporation, “Part and Mold Design.,” p. 168, 2007.
- [10] M. T. Standards, “Technical product information,” vol. 102, no. 0, pp. 2–3, 1800.
- [11] T. Garbacz, T. Jachowicz, I. Gajdoš, and G. Kijewski, “Research on the Influence of Blowing Agent on Selected Properties of Extruded Cellular Products,” *Adv. Sci. Technol. Res. J.*, vol. 9, no. 28, pp. 81–88, 2015.

- [12] D. L. Michelson, L. W. B. Charlotte, J. Robert, and C. Mt, "United States Patent 09] Date of Patent :," no. 19, pp. 1–6, 1998.
- [13] M. Gringras, "United States Patent Office," *J. Am. Soc. Nav. Eng.*, vol. 39, no. 4, pp. 620–622, 2009.
- [14] "injection-moulding-for-auto-parts @ www.acomold.com." [Online]. Available: <http://www.acomold.com/injection-moulding-for-auto-parts.html>.
- [15] A. Rogić, I. Čatić, and D. Godec, *Polimeri i polimerne tvorevine*. Zagreb: Biblioteka polimerstvo, 2008.
- [16] R. A. Malloy, "Case_General @ Www.Me.Umn.Edu," 1994. [Online]. Available: http://www.me.umn.edu/~kstelson/research_sbp/sbp/case/case_general.html.
- [17] I. Čatić, N. Razi, and P. Raos, *Analiza injekcijskog pređanja polimera teorijom sustava*. Zagreb: Društvo plastičara i gumaraca, 1991.
- [18] "Industrial_computed_tomography @ en.wikipedia.org." .
- [19] K. J. Batenburg, C. Hansen, J. S. Jørgensen, and W. R. B. Lionheart, *Scientific Computing for Computed Tomography*. Copenhagen: DTU, 2018.
- [20] A. Cantatore and P. Muller, *Introduction to computed tomography*. Kgs.Lyngby:DTU Mechanical Engineering, 2011.
- [21] R. Hanke, T. Fuchs, and N. Uhlmann, "X-ray based methods for non-destructive testing and material characterization," *Nucl. Instruments Methods Phys. Res. Sect. A Accel. Spectrometers, Detect. Assoc. Equip.*, vol. 591, no. 1, pp. 14–18, 2008.
- [22] "Godfrey_Hounsfield @ en.wikipedia.org," 2019. [Online]. Available: https://en.wikipedia.org/wiki/Godfrey_Hounsfield.
- [23] S. Brown and R. Leach, "NPL REPORT ENG 32 An overview of industrial X-ray computed tomography Sun W, Brown S B and Leach R K JANUARY 2012," *Measurement*, no. January, 2012.
- [24] "volume-pixel-volume-pixel-or-voxel @ www.techopedia.com," 2019. [Online].

- Available: <https://www.techopedia.com/definition/2055/volume-pixel-volume-pixel-or-voxel>.
- [25] S. Siddique *et al.*, “Computed tomography for characterization of fatigue performance of selective laser melted parts,” *Mater. Des.*, vol. 83, pp. 661–669, 2015.
- [26] G. Nikishkov, Y. Nikishkov, and A. Makeev, “Finite element mesh generation for composites with ply waviness based on X-ray computed tomography,” *Adv. Eng. Softw.*, vol. 58, pp. 35–44, 2013.
- [27] S. J. Kim, C. S. Lee, H. J. Yeo, J. H. Kim, and J. Y. Cho, “Direct numerical simulation of composite structures,” *J. Compos. Mater.*, vol. 36, no. 24, pp. 2765–2785, 2002.
- [28] S. J. Kim, K. H. Ji, and S. H. Paik, “Numerical simulation of mechanical behavior of composite structures by supercomputing technology,” *Adv. Compos. Mater.*, vol. 17, no. 4, pp. 373–407, 2008.
- [29] J. Y. Cho, J. H. Kim, C. S. Lee, and S. J. Kim, “Determination of Composite Material Constants By Direct Numerical Simulation.”
- [30] “Digimat User Manual,” no. August, 2014.